



THE UNIVERSITY *of* EDINBURGH

Edinburgh Research Explorer

Cyclin A and Cks1 promote kinase consensus switching to non-proline-directed CDK1 phosphorylation

Citation for published version:

al-Rawi, A, Kaye, E, Korolchuk, S, Endicott, JA & Ly, T 2023, 'Cyclin A and Cks1 promote kinase consensus switching to non-proline-directed CDK1 phosphorylation', *Cell Reports*, vol. 42, no. 3, 112139, pp. 112139. <https://doi.org/10.1016/j.celrep.2023.112139>

Digital Object Identifier (DOI):

[10.1016/j.celrep.2023.112139](https://doi.org/10.1016/j.celrep.2023.112139)

Link:

[Link to publication record in Edinburgh Research Explorer](#)

Document Version:

Publisher's PDF, also known as Version of record

Published In:

Cell Reports

General rights

Copyright for the publications made accessible via the Edinburgh Research Explorer is retained by the author(s) and / or other copyright owners and it is a condition of accessing these publications that users recognise and abide by the legal requirements associated with these rights.

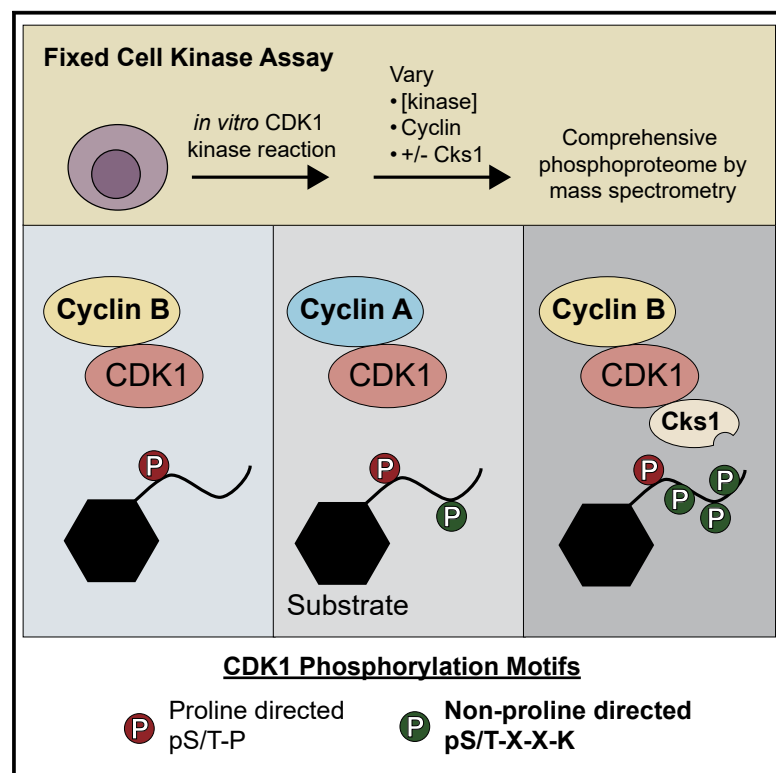
Take down policy

The University of Edinburgh has made every reasonable effort to ensure that Edinburgh Research Explorer content complies with UK legislation. If you believe that the public display of this file breaches copyright please contact openaccess@ed.ac.uk providing details, and we will remove access to the work immediately and investigate your claim.



Cyclin A and Cks1 promote kinase consensus switching to non-proline-directed CDK1 phosphorylation

Graphical abstract



Authors

Aymen al-Rawi, Edward Kaye, Svitlana Korolchuk, Jane A. Endicott, Tony Ly

Correspondence

tly@dundee.ac.uk

In brief

Cyclin-dependent kinase (CDK) substrate phosphorylation varies in a cell-cycle-dependent manner. al-Rawi et al. develop a fixed cell kinase assay to study CDK1 kinase substrate choice proteome-wide in human cells. This reveals an alternative, non-proline-directed consensus sequence for CDK1, [S/T][P]XK, that is regulated by CDK1 complex composition.

Highlights

- A proteome-wide assay was developed to study CDK1 kinase substrate choice
- CDK1 can phosphorylate an alternative [S/T][P]XK consensus sequence
- Most mitotic phosphorylation sites are CDK1 substrates *in vitro*
- Cks1 is self-primed by CDK1 and promotes proteome-wide multisite phosphorylation



Article

Cyclin A and Cks1 promote kinase consensus switching to non-proline-directed CDK1 phosphorylation

Aymen al-Rawi,^{1,2} Edward Kaye,¹ Svitlana Korolchuk,³ Jane A. Endicott,^{3,4} and Tony Ly^{1,2,5,*}
¹Centre for Gene Regulation and Expression, School of Life Sciences, University of Dundee, Dundee DD1 5EH, UK

²Wellcome Centre for Cell Biology, School of Biological Sciences, University of Edinburgh, Edinburgh EH9 3BF, UK

³Medical School, Newcastle University, Newcastle upon Tyne NE2 4HH, UK

⁴Translational and Clinical Research Institute, Faculty of Medical Sciences, Newcastle University, Newcastle upon Tyne NE2 4HH, UK

⁵Lead contact

*Correspondence: tly@dundee.ac.uk
<https://doi.org/10.1016/j.celrep.2023.112139>

SUMMARY

Ordered protein phosphorylation by CDKs is a key mechanism for regulating the cell cycle. How temporal order is enforced in mammalian cells remains unclear. Using a fixed cell kinase assay and phosphoproteomics, we show how CDK1 activity and non-catalytic CDK1 subunits contribute to the choice of substrate and site of phosphorylation. Increases in CDK1 activity alter substrate choice, with intermediate- and low-sensitivity CDK1 substrates enriched in DNA replication and mitotic functions, respectively. This activity dependence is shared between Cyclin A- and Cyclin B-CDK1. Cks1 has a proteome-wide role as an enhancer of multisite CDK1 phosphorylation. Contrary to the model of CDK1 as an exclusively proline-directed kinase, we show that Cyclin A and Cks1 enhance non-proline-directed phosphorylation, preferably on sites with a +3 lysine residue. Indeed, 70% of cell-cycle-regulated phosphorylations, where the kinase carrying out this modification has not been identified, are non-proline-directed CDK1 sites.

INTRODUCTION

Ordered phosphorylation by cyclin-dependent kinases (CDKs) controls the timing and progression of the cell division cycle. Temporal regulation of CDK phosphorylation is critical, ensuring that DNA replication origin licensing, DNA replication, and chromosome segregation occur in sequential order.^{1–3} CDK1 is essential to embryonic cell division and supports cell division in the absence of interphase CDKs (CDK2/4/6).⁴ In *S. pombe*, a single cyclin-CDK fusion can drive a relatively unperturbed cell cycle in optimal growth conditions.⁵ How temporal ordering of CDK1 phosphorylation is controlled in mammalian cells remains a major open question.

Complex formation with a cognate cyclin is requisite to CDK activation. Mouse knockout studies have shown the differential requirements of cyclins and CDKs in embryogenesis and development.^{4,6} However, understanding how CDK phosphorylation is controlled in mammalian cells is challenging because of redundancy in the cyclin-CDK family and kinase-phosphatase feedback loops (e.g., Wee1/Cdc25, Greatwall/PP2A-B55) that can be acutely sensitive to changes in CDK activity in cells.^{7–11}

Cks is a third subunit found in active cyclin-CDK complexes that is conserved from yeast (Suc1 in *S. pombe*) to human. Cks1 acts as a phosphoadaptor protein with selectivity for phosphothreonine.¹² Mammalian genomes encode two Cks proteins (CKS1B and CKS2), and deletion of both results in embryonic

lethality.¹³ Cks1 (encoded by CKS1B), but not Cks2, promotes the ubiquitination and degradation of the CDK inhibitor protein p27^{KIP} and promotes cell-cycle entry.^{14,15} In *S. cerevisiae*, Cks1 facilitates multisite phosphorylation of the CDK substrate protein Sic1.¹⁶ Docking of Cks1 onto priming sites is thought to promote the phosphorylation of low-affinity sites by *cdc28* (CDK1 in human).¹⁷ It is unclear how many CDK substrates require Cks1 for high-occupancy phosphorylation.

In *S. pombe*, a quantitative model of CDK1 substrate choice was proposed whereby substrates with functions in DNA replication have lower thresholds for CDK1 phosphorylation than substrates with functions in mitosis.^{18,19} Thus, temporal ordering is achieved by a progressive increase in CDK1 activity. In *S. cerevisiae*, qualitative differences, for example in the cyclin subunit, confer substrate specificity to CDK1.^{20–22} Cyclins E, A, and D have a hydrophobic patch ~35 Å from the catalytic site that has been shown to be important in substrate recognition by binding to a Cy motif (RXL, where X is any amino acid) in disordered regions.^{23–26} Mutation of the hydrophobic patch significantly reduces phosphorylation occupancy for a subset of substrates. The hydrophobic patch is not completely degenerate between cyclins because identical mutations have differential effects on substrate phosphorylation dependent on the cyclin subunit.²⁰ Additionally, cyclins are targeted to distinct subcellular compartments.^{27–29} This targeting is encoded in nuclear localization and export sequences that differ between cyclins. Consistent with these results, cyclins have



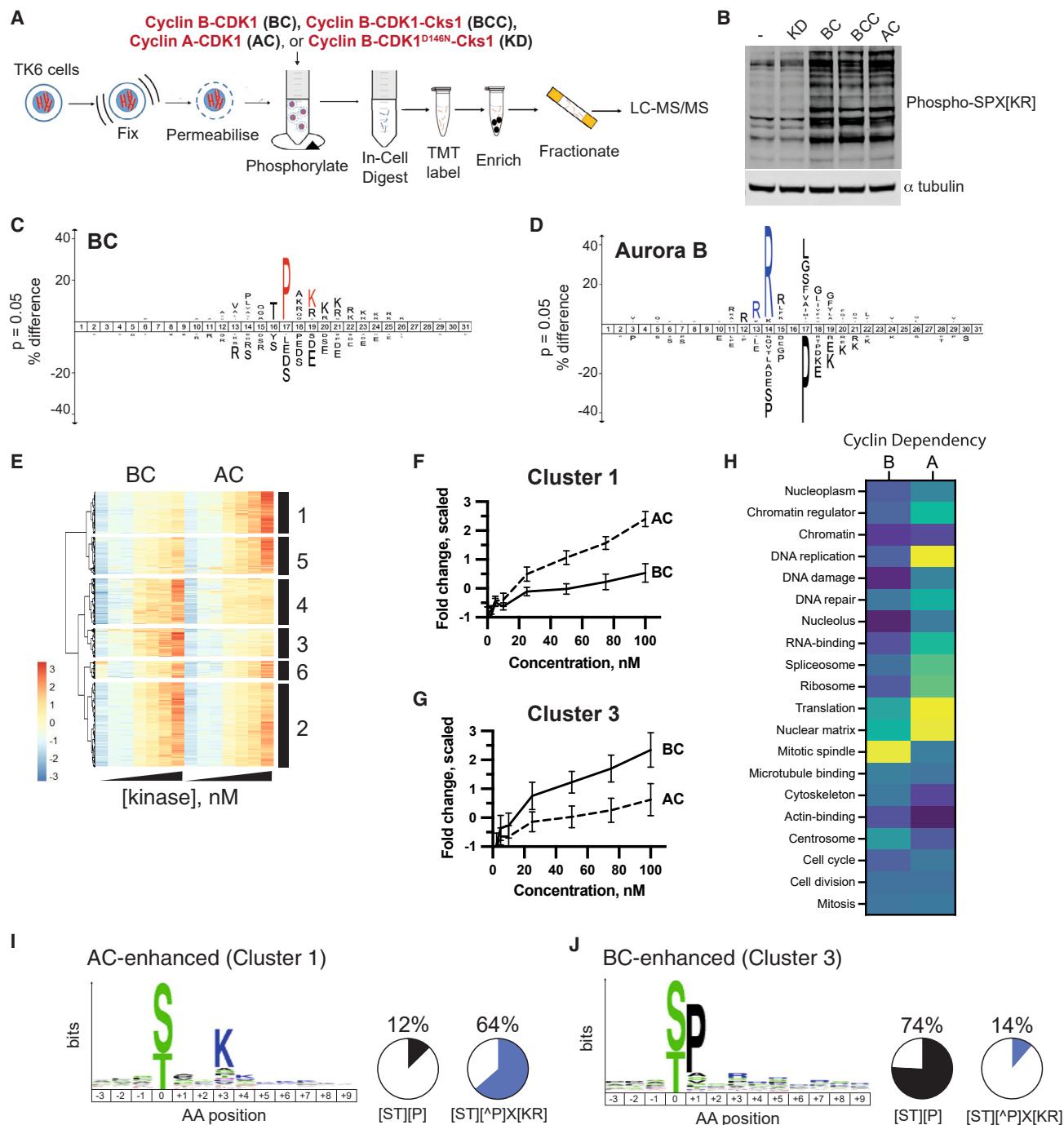


Figure 1. Cyclin A2 promotes non-proline-directed CDK1 phosphorylation and modulates substrate specificity *in vitro*

(A) Scheme of the *in vitro* kinase assay on fixed cells. Cyclin B1-CDK1 (BC), Cyclin B1-CDK1-Cks1 (BCC), Cyclin A2-CDK1 (AC), and a kinase-dead mutant of CDK1, Cyclin B1-CDK1^{D146N}-Cks1 (KD), were compared.

(B) Western blot of lysates from fixed cells phosphorylated using the assay described in (A) with anti-phospho-SPX[KR] motif antibody, which also crossreacts with phosphorylated MAPK motifs, i.e., PXPSP.

(C) Motif enrichment analysis of fixed G2/M cells phosphorylated by either BC or BCC CDK1 complexes. Amino acids shown on top and bottom are enriched and under-represented, respectively, in kinase phosphorylated sites, compared with background.

(D) Motif enrichment analysis of fixed G2/M cells phosphorylated by Aurora B.

(legend continued on next page)

overlapping and complementary interaction partners in cells.³⁰ Cyclins also have non-redundant functions. Cyclin A2 is essential for mitotic entry and prevents hyperstable kinetochore-microtubule attachments in early mitosis.^{10,31,32} In contrast, cells depleted of Cyclin B proteins progress into mitosis but fail to complete proper chromosome segregation.¹⁰

CDK1 phosphorylation of individual sites on a substrate protein is ordered to produce ultrasensitive switches in protein function.³³ However, little is known about how this order is regulated. Phosphorylation site choice within a substrate is determined by molecular interfaces proximal to the catalytic site. A structure for Cyclin A-CDK2 in complex with a peptide substrate shows that a substrate binding cleft formed on one side by the activation loop imposes a preference for a proline in the +1 position and a basic residue in the +3 position,^{34,35} which is consistent with data from peptide arrays.³⁶ Compared with CDK2, the activation loop of CDK1 is more flexible, possibly allowing for a relaxed consensus requirement.³⁴ By contrast, under the same reaction conditions, CDK2 is unable to phosphorylate these “non-canonical” CDK sites. Non-canonical CDK1 sites have been described for individual protein substrates and for substrates in mouse embryonic stem cells (mESCs).^{17,37,38,39} However, it is unknown what proportion of the CDK substrate phosphorylations are on non-canonical sites and if and how non-canonical phosphorylations are regulated.

Recent advances in mass spectrometry (MS)-based proteomics have enabled quantitative and comprehensive analysis of cellular protein phosphorylation.^{40–42} These approaches have produced an extensive catalog of phosphorylation sites in human cells that are cell-cycle regulated, recently with high temporal resolution.⁴³ Many cell-cycle-regulated phosphorylation sites do not match any known kinase consensus sequence,⁴¹ leading to speculation that there are unknown kinases that drive a significant fraction of cell-cycle-regulated phosphorylations.

In this study, we developed an *in vitro* approach to investigate how quantitative and qualitative characteristics of the CDK1 complex contribute to substrate choice and phosphorylation. Fixed and permeabilized cells are subjected to kinase reactions with recombinant CDK1 in complex either with Cyclin B, Cyclin A, or Cyclin B-Cks1. We show that both Cyclin A2 and Cks1 promote the phosphorylation of non-proline sites by CDK1 *in vitro*. Cyclin A2-CDK1 non-proline-directed sites are enriched in a lysine in the +3 position (+3K) in a motif defined by [ST][P]X[KR], where [P] indicates any residue except for proline. CDK1 sites detected *in vitro* are cell-cycle regulated *in vivo*, including non-proline-directed sites and sites containing the +3K motif. By combining sequential enzymatic reactions on fixed cells, we demonstrate that the majority of Cks1-promoted sites are primed by CDK1 itself. Based on our data, we propose a model whereby the non-catalytic CDK1 subunits determine substrate specificity and phosphoacceptor residue choice, while the role

of Cks1 is an enhancer of cyclin-CDK1 activity by promoting multisite phosphorylation.

RESULTS

A fixed cell kinase assay to investigate substrate phosphorylation proteome-wide *in vitro*

To investigate the role of the Cks1 and the cyclin subunits in CDK1 substrate phosphorylation, we designed an *in vitro* kinase assay in which formaldehyde-fixed and methanol-permeabilized TK6 cells are incubated with purified CDK1 in complex with either Cyclin B1 (BC), Cyclin B1 and Cks1 (BCC), or Cyclin A2 (AC) (Figure 1A). CDK1 was shown to be sufficient to drive cell-cycle progression in the absence of the interphase CDKs *in vivo*.⁴ Therefore, we used centrifugal elutriation to enrich for cells in the G2/mitotic (M) phases of the cell cycle (fractions 11 and 12 in Figure S1A). In these cells, targets of interphase CDKs (CDK2/4/6) will be phosphorylated, and protein substrates critical to the essential role of CDK1 in mitotic entry are expressed. Increased phosphorylation on SPX[KR] motifs was observed after reaction with complexes containing active CDK1, but not a kinase-dead CDK1 mutant (CDK1^{D146N}, KD) (Figure 1B). Phosphorylation is a readout for two molecular events: an interaction between the recombinant CDK1 added and the substrate and catalytic phosphotransfer. Because cells are fixed and phosphatase/kinase activities are largely suppressed (Figures S1B–S1D), phosphorylation detected in our assays is direct and not subject to feedback (e.g., via Greatwall-Arpp19/ENSA^{44,45}). We then prepared peptide digests from the phosphorylated cells using an in-cell digest.⁴⁶ Peptide digests were labeled with 16-plex tandem mass tags (TMTs), enriched for phosphorylated peptides, fractionated offline by high-performance liquid chromatography (HPLC) prior to LC coupled tandem MS (LC-MS/MS) analysis (Figure 1A). 3,377 phosphorylation sites, representing 2,493 proteins, were increased by 2-fold or more compared with KD. Motif enrichment analysis of significantly changing phosphorylation sites revealed a known consensus sequence for CDK1 (TPXK) (Figure 1C). In contrast, sites significantly increased after treatment with Aurora B are enriched in an RRX[ST] motif (Figure 1D). Our results recapitulate consensus motifs obtained using cell-based assays,^{47,48} indicating that sites identified in fixed cell assays are specific to the kinase added.

AC shifts the substrate specificity of CDK1 and promotes the phosphorylation of non-proline sites *in vitro*

To investigate how the quality and quantity of CDK1 affect substrate choice, we used the fixed cell assays described above to measure CDK1 substrate phosphorylation proteome-wide comparing AC and BC titrated from 2.5 to 100 nM recombinant

(E) Fixed G2/M cells were titrated with increasing concentration of either AC or BC and subjected to phosphoproteomic analysis. Color indicates the scaled fold change relative to KD.

(F and G) The mean fold change plotted against the concentration of AC and BC for cluster 1 (F) or 3 (G). Error bars represent the standard deviation.

(H) Heatmap showing fold enrichment for selected Gene Ontology (GO) terms and UniProt keywords comparing Cyclin A- versus Cyclin B-dependent phosphorylation sites.

(I and J) Motif enrichment analysis of sites from cluster 1 (I) or 3 (J). Proportion of sites matching +1 proline (proline directed, black) or [ST][P]X[KR] (blue) motifs, where P denotes any amino acid besides proline and X is any amino acid.

kinase. An upper limit of 100 nM was chosen based on estimated copies of BC and CDK1 detected in G2/M-phase leukemic cells.^{49,50} 27,084 phosphorylation sites were detected, of which 5,113 sites changed by 2-fold or more compared with KD-treated cells (Table S1). This dataset allowed us to investigate how increasing CDK1 activity quantity affects substrate choice by measuring concentration-dependent changes in substrate phosphorylation. On the other hand, with the same dataset, we can investigate how the quality of CDK1 activity (i.e., the different cyclin subunit) impacts substrate choice.

To assess the relative differences between Cyclin A and Cyclin B phosphorylation for the same site, fold changes were scaled (see STAR Methods) and normalized for differences in kinase activity between recombinant kinase preparations (Figures S1E and S1F) using histone H1 as the prototypical substrate (e.g., Loog and Morgan²⁰). Next, we investigated the subcellular localization of the added recombinant kinases. Kinase-treated cells were fixed again with formaldehyde and immunostained for CDK1. No significant differences between AC, BC, and BCC were observed in the ratio of nuclear-to-cytoplasmic CDK1 signal, suggesting that the localizations of recombinant complexes added were similar (Figure S1G). In contrast, *in vivo*, active nucleocytoplasmic transport restricts BC to the cytoplasm and AC to the nucleus prior to nuclear envelope breakdown.⁵¹ Thus, any differences in substrate phosphorylation by AC and BC observed in the subsequent analysis are not due to variation in kinase activity or subcellular localization of the added kinase and instead are due to qualitative differences conferred by the cyclin subunit.

Hierarchical clustering was used to identify groups of phosphorylation sites that exhibited similar patterns of phosphorylation. This clustering identified six major clusters of phosphorylation sites (Figure 1E). Sites in cluster 1 were phosphorylated to a higher extent with AC compared with BC and therefore are Cyclin A dependent (Figure 1F). Vice versa, sites in cluster 3 were Cyclin B dependent (Figure 1G).

Are there characteristics that distinguish Cyclin A- versus Cyclin B-dependent phosphorylation sites and substrate proteins? To address this question, we compared clusters 1 and 3 because they show the most extreme differences in cyclin dependence and assessed functional annotations (Figure 1H). Cyclin A-dependent protein substrates were differentially enriched in proteins with functions in DNA replication, protein translation, and proteins localized to the nuclear matrix. In contrast, Cyclin B-dependent protein substrates were enriched in proteins localized to the mitotic spindle and centrosomes. Cyclin A- and Cyclin B-dependent substrates were equally enriched in proteins with functions in mitosis and cell division (Figure 1H, bottom). No significant difference was observed between Cyclin A- versus Cyclin B-dependent substrates in whether they contain 1 or more RXL motifs in the same disordered region as the phosphorylation site (Fisher's exact test, $p > 0.05$).

Cyclin A-dependent sites show a remarkable depletion of proline in the +1 position, with only 12% of sites being proline directed (Figure 1I). In contrast, Cyclin B-dependent sites show a strong +1 proline (+1P) preference, with 74% sites being proline directed (Figure 1J). Cyclin A-dependent sites contain a

prominent enrichment of lysine at the +3K (Figure 1I). 64% of Cyclin A-dependent sites meet the [ST][P]X[KR] motif (Figure 1I). In contrast, 14% of Cyclin B-dependent sites meet this [ST][P]X[KR] motif (Figure 1J).

We conclude that the cyclin subunit has a major role in substrate targeting. Cyclin A increases the frequency of non-proline-directed CDK1 phosphorylation compared with Cyclin B, and these sites are enriched in the [ST][P]X[KR] motif.

Quantitative increases in CDK1 activity alter substrate specificity *in vitro*

Phosphorylation does not saturate in the range of kinase concentrations tested (Figure 1E), which may contribute to the lack of obvious clusters of phosphorylation sites that differ in concentration dependence (Figure 1E). For many sites, phosphorylation is not detected in KD-treated cells, therefore making exact fold changes challenging to accurately estimate. Therefore, to facilitate comparison of concentration dependence between sites, an arbitrary fold change cap was used to enforce phosphorylation saturation *in silico*. A cap of 6.5 was chosen because this was the median fold change for phosphorylation sites increased in M versus G2 cells. This approach enables us to determine if, and at what concentration, the phosphorylation effectively reaches the median fold change observed in the G2-to-M transition in cells.

Using this strategy, we identified seven clusters of phosphorylation sites that differed in BC concentration dependence (Figures 2A and 2B; Table S2). Cluster 1 shows fold changes of 6.5 or more at 2.5 nM, the lowest concentration tested. At the other extreme, sites in cluster 7 do not reach fold changes of 6.5 or more at 100 nM and follow a linear response to kinase concentration. Proteins in these clusters were then subjected to functional gene annotation enrichment analysis. Figure 2C shows selected functional Gene Ontology (GO) annotations that show a significant (false discovery rate [FDR] < 0.01) in one or more clusters. Cluster 1 shows no major differential enrichment. Interestingly, cluster 2 shows an enrichment in proteins associated with protein translation, including ribosomal proteins. Sites with moderate sensitivity to CDK1 activity (cluster 4) are significantly enriched in proteins involved in DNA repair and DNA replication. Sites with lower CDK1 sensitivity (cluster 6) are enriched in proteins involved in the organization of the mitotic spindle, chromosome segregation, and nuclear envelope disassembly. For example, proteins in cluster 6 show a 7.6-fold enrichment in mitotic spindle assembly proteins, which is three times higher than cluster 1. Similar trends in clustering and functional enrichment are observed with AC (Figures S2A–S2C). Individual CDK1 substrate proteins may have sites belonging to multiple clusters. Indeed, 943 out of 2,550 CDK1 substrate proteins have phosphorylation sites with differing sensitivities to CDK1 phosphorylation. CDK1 phosphorylation sites on these substrates represent the majority of the phosphorylation sites (64%, 3,288/5,113). We conclude that quantitative changes in the activities of Cyclin A-CDK1 and Cyclin B-CDK1 alter substrate specificity in a similar concentration-dependent manner, with many substrates having multiple CDK1 sites with differing sensitivities to kinase activity.

We next assessed if clusters differed in amino acid sequence proximal to the phosphoacceptor residue. Low- and

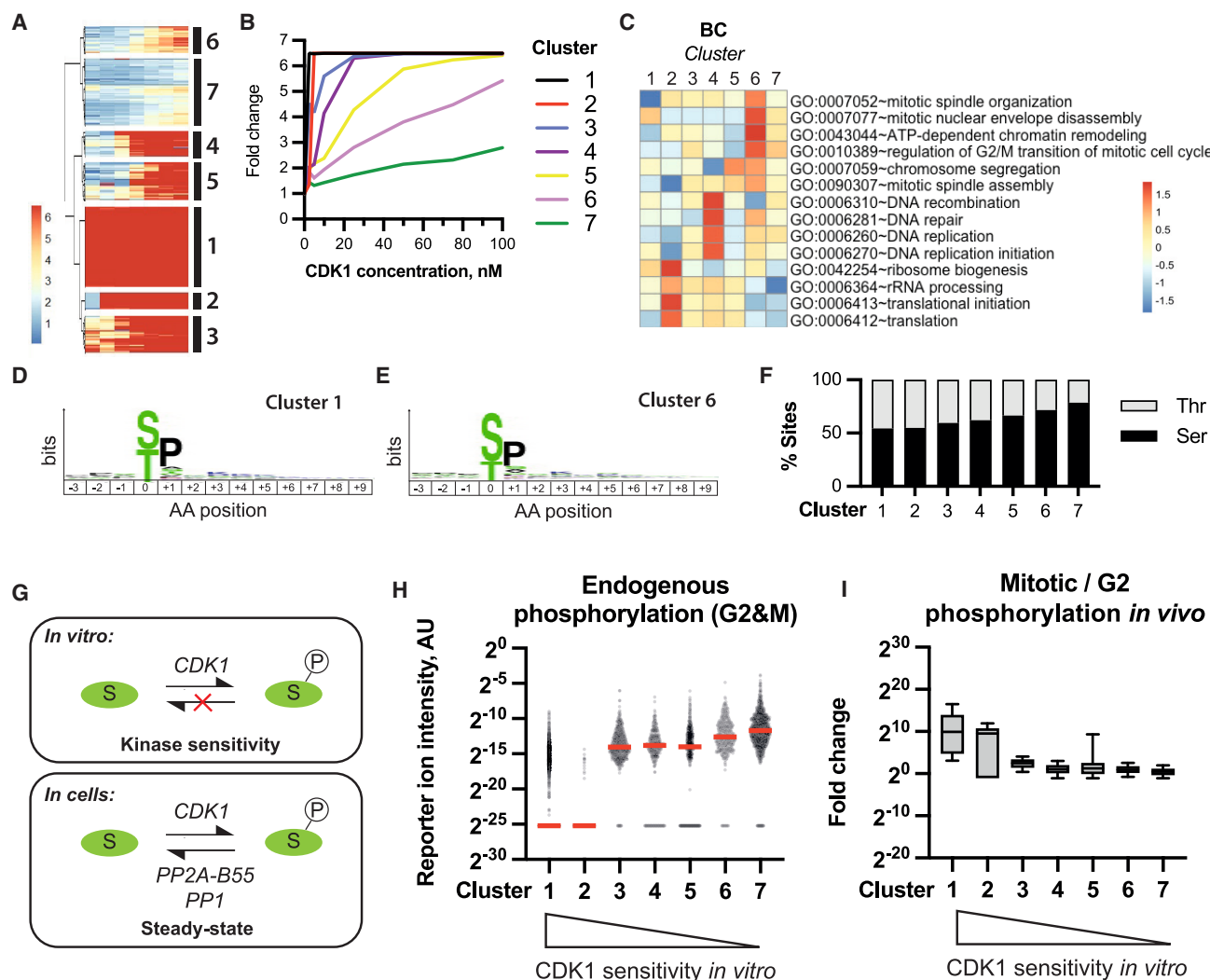


Figure 2. Quantitative increases in CDK1 activity alter substrate specificity *in vitro*

(A) G2/M cells were titrated with increasing concentrations of KD or BC and subjected to phosphoproteomic analysis. Heatmap showing the capped fold changes against KD. Hierarchical clustering identified seven clusters.

(B) Mean capped fold change versus CDK1 concentration for each cluster.

(C) Scaled fold enrichment for selected enriched GO terms.

(D and E) Motif analysis of sites in clusters 1 (D) and 6 (E).

(F) Proportion of serine and threonine phosphoacceptor residues per cluster.

(G) Model for the readout of phosphorylation in fixed cells (kinase sensitivity) versus in viable cells (steady-state levels, which are subject to kinase-phosphatase antagonism).

(H) Normalized phosphopeptide intensities detected in KD-treated G2/M cells (i.e., the endogenous phosphorylation in cells) per cluster. Bars indicate medians.

(I) Fold-change comparing mitotic (STLC-arrested) versus G2/M-phase cells per cluster. Bars indicate medians, and box and whiskers show 75th/25th and 90th/10th percentiles, respectively.

high-CDK1-sensitivity clusters showed a similar preference for +1P (Figures 2D and 2E). Similar results were obtained using Cyclin A-CDK1 (Figure S2B). Interestingly, high-CDK1-sensitivity sites in cluster 1 have a high proportion of threonine phosphoacceptor sites (~50%, Figure 2F). In contrast, the proportion of threonine sites (over serine) is 36% and 23% for CDK1 sites and all detected sites, respectively. Indeed, the proportion of threonine phosphoacceptor residues is negatively correlated with CDK1 concentration dependence (Figure 2F).

In the fixed cell assay, substrate phosphorylation will be determined solely by the forward kinase reaction. However, in living cells, substrate phosphorylation will be subject to antagonism by cellular protein phosphatases, including PP2A:B55 and PP1, as illustrated in Figure 2G. PP2A:B55 has been shown to prefer dephosphorylating phosphothreonine residues with a +1P and is active in interphase.^{52–54} Could targeted dephosphorylation by PP2A:B55 *in vivo* lead to lower occupancy of TP sites in fixed G2 cells? To address this question, we examined

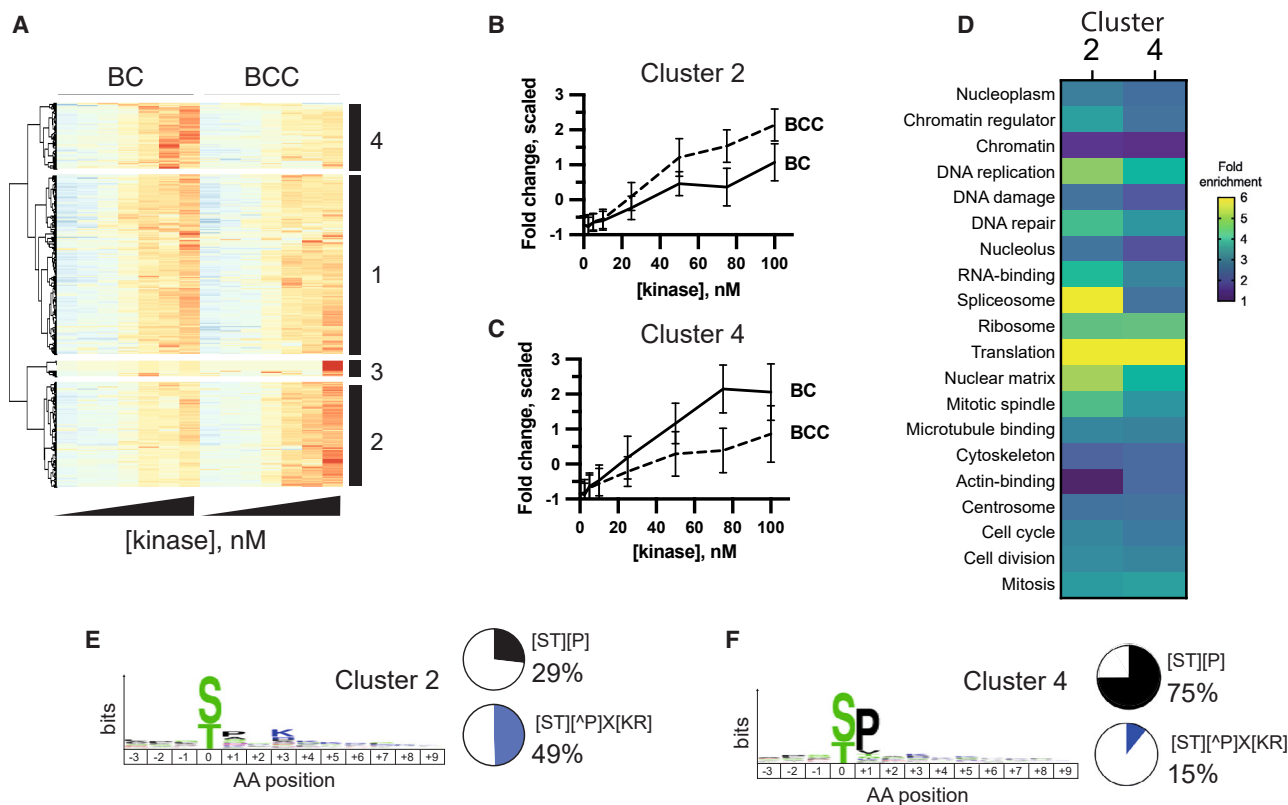


Figure 3. Cks1 promotes widespread phosphorylation of non-proline-directed sites by human Cyclin B-CDK1 *in vitro*

(A) G2/M cells were titrated with increasing concentrations of KD, BC, or BCC and subjected to phosphoproteomic analysis. Heatmap showing the scaled fold changes against KD. Hierarchical clustering was used to identify Cks1-enhanced (cluster 2) and Cks1-inhibited (cluster 4) phosphorylation sites. (B and C) Line graphs showing mean fold change for clusters 2 (B) and 4 (C). Error bars represent the standard deviation. (D) Heatmap showing fold enrichment for selected GO terms and UniProt keywords comparing Cks1-enhanced versus Cks1-inhibited phosphorylation sites. (E and F) Motif analysis of the sites in clusters 2 (E) and 4 (F) using WebLogo. Pie charts show the proportions of sites in the cluster with the indicated motif, e.g., +1P (black) or [ST][^P]X[KR] (blue), where 'P' denotes any amino acid besides proline and X is any amino acid.

the endogenous abundance of phosphorylation in G2/M cells, grouped into phosphorylation sites determined by CDK1 sensitivity *in vitro* (Figure 2H). Cluster 1 has the highest proportion of threonine sites and the lowest level of endogenous phosphorylation. Indeed, there is a negative correlation between CDK1 sensitivity *in vitro* and the median level of endogenous phosphorylation (Figure 2H). Within a cluster, however, individual sites range widely in levels of endogenous phosphorylation (Figure 2H), suggesting that the sensitivity toward CDK1 *in vitro* is unlikely to be driven exclusively by endogenous occupancy. Consistent with this idea, differences in CDK1 sensitivity *in vitro* persist in reactions of fixed cells pre-treated with lambda phosphatase (Figure S2D) while showing no significant difference in serine versus threonine phosphoacceptor frequency (Figure S2E). Is CDK1 sensitivity *in vitro* reflected *in vivo*? To test this, we plotted endogenous phosphorylation fold changes comparing M and G2 cells because, in mitosis, PP2A:B55 is inactivated, and CDK1 activity is high. Indeed, sites showing the highest sensitivity to CDK1 *in vitro* show the highest fold changes in mitosis (Figure 2I). These data support a model whereby phosphatase inactivation is a crucial determinant of CDK1 substrate phosphorylation.^{44,45,55,56}

Cks1 promotes the phosphorylation of non-proline sites by CDK1 *in vitro*

To assess the role of Cks1 in BC-CDK1 interaction with cellular substrates, we titrated fixed G2/M-enriched TK6 cells with increasing concentrations of either BC or BCC, performed in biological duplicate. Out of 24,139 sites identified (Table S3), 3,377 sites showed a 2-fold or more increase in phosphorylation upon addition of active CDK1. Note that the data for BC are identical to that shown in Figure 1. Fold changes were normalized for differences in CDK1 activity, as above (Figure S3A). Individual sites differed in CDK1-concentration dependence (Figure 3A), and some sites were phosphorylated to higher extent with BCC compared with BC, and vice versa. Phosphorylation sites were separated into four clusters by hierarchical clustering. Phosphorylation sites in cluster 2 show strong enhancement by the Cks1 subunit (Figure 3B). The remaining sites were either phosphorylated to a greater extent by BC (cluster 4; Figure 3C; "Cks1-inhibited cluster") or equally phosphorylated by BC and BCC (cluster 1). Interestingly, there is a small set of phosphorylation sites that are highly phosphorylated by BCC at 100 nM kinase (cluster 3).

How do Cks1-enhanced sites differ from Cks1-inhibited ones? A functional enrichment analysis was performed comparing

clusters 2 and 4. In general, the differences seen between Cks1-enhanced and Cks1-inhibited substrates (Figure 3D) are less than those observed between Cyclin A-CDK1 and Cyclin B-CDK1. Splicing factors, however, are a striking exception, being highly enriched in Cks1-enhanced substrates. Enrichment is also slightly higher in Cks1-enhanced substrates for proteins localized to the nuclear matrix and with functions in DNA replication. These results support a model whereby BCC increases phosphorylation of a subset of BC substrates.

We next tested if the local amino acid sequence around the phosphoacceptor site in the Cks1-enhanced cluster (cluster 2) is significantly different from a Cks1-inhibited cluster (cluster 4). As shown in Figure 3E, Cks1-enhanced sites are depleted of +1P. Strikingly, only 29% of Cks1-enhanced sites had a +1P, in contrast to Cks1-inhibited sites, in which 75% were proline directed (Figure 3F). There is a slight preference for +3K but less than Cyclin A-dependent sites (Figure 1I). 49% of Cks1-enhanced sites are within a [ST][P]X[KR] motif. In contrast, only 15% of Cks1-inhibited sites meet this consensus (Figure 3F). We conclude that Cks1 has a proteome-wide role in promoting CDK1 phosphorylation of non-proline-directed sites *in vitro*.

Cks1 enhances CDK1-primed multisite phosphorylation of substrate proteins *in vitro*

Cks1 enhances multisite phosphorylation of *S. cerevisiae* Sic1 by phosphodependent docking to a priming site.^{16,17} It was proposed that Cks1 acts as a molecular ruler by promoting the phosphorylation of a second-site 12–15 amino acid C-terminal to the priming site (Figure 4A). To what extent does phosphate docking play a role in CDK1 phosphorylation in human cells? And is this role of Cks1 proteome-wide?

We reasoned that if Cks1 promoted multisite phosphorylation, then Cks1-enhanced protein substrates should show, on average, a higher number of sites phosphorylated by CDK1 *in vitro* than Cks1-inhibited substrates. Indeed, Cks1-enhanced substrates had on average two CDK1 phosphorylation sites per protein (median) compared with one site per protein for Cks1-inhibited substrates (Figure 4B). Many proteins had multiple sites, some that were Cks1 enhanced and others that were Cks1 inhibited. For example, on the protein Ki-67, 49 sites are phosphorylated by CDK1 in total, of which 24 are Cks1 enhanced. Unlike Cks1, the cyclin subunit does not alter multisite substrate phosphorylation (Figure S3B).

Next, we examined the distribution of secondary phosphorylation sites surrounding a Cks1-dependent phosphoacceptor site, reasoning that if Cks1 acts as a molecular ruler, we should observe “hot spot” of secondary phosphorylation. In support of this model, secondary phosphorylation sites are enhanced at positions –15 and +12 for BCC-dependent non-proline sites (Figure 4C). Interestingly, proline-directed CDK1 sites overall do not show this behavior (Figure 4D). The enhancement is seen for both serine and threonine phosphoacceptor residues, and there is no difference in pattern if the secondary is restricted to either serine or threonine. Interestingly, there is a depletion of secondary phosphorylation sites from positions –8 to +6 for BCC-dependent non-proline sites compared with proline-directed sites. These results support a model whereby Cks1

docks onto a proximal priming site to facilitate multisite phosphorylation, frequently at non-proline-directed sites.

The identity of the major priming kinase for Cks1 is unknown. In *S. cerevisiae*, CDK-Cks complexes can self-prime to phosphorylate a substrate in a processive manner.¹⁷ To investigate the Cks1 priming kinase, we designed an experiment combining sequential phosphatase and kinase reactions on fixed cells. We reasoned that removal of all endogenous phosphorylation in G2 cells would eliminate priming by all kinases except for the one added (CDK1). By using a proteome-wide approach, we can identify which Cks1-dependent sites are dependent on priming by CDK1 or by other kinases (Figure 4E).

TK6 cells were treated with λ phosphatase, followed by BCC. Phosphatase pre-treatment eliminated endogenous SPX[KR] phosphorylation (Figure 4F, lanes 1 and 6), and SPX[KR] phosphorylation is increased after treatment with BC or BCC (Figure 4F, e.g., compare lanes 2 and 3). Reactions were then analyzed by LC-MS/MS as shown in Figure 1A. 23,911 sites were identified, of which 5,819 sites were phosphorylated by CDK1 (G2/M cells; Table S4). Sites phosphorylated by CDK1 in mock-treated cells were clustered (Figure 4G) to identify Cks1-enhanced sites (Figures 4G, arrow, and 4H). We then asked if these sites were phosphorylated by CDK1 in λ phosphatase-treated cells. Of the 1,013 Cks1-enhanced sites phosphorylated in mock-treated cells, 873 sites showed a 2-fold or higher change after addition of BCC to λ phosphatase-treated cells compared with KD (Figure 4I). This result demonstrates that CDK1 has priming activity for most Cks1-dependent sites (86%). The remaining 140 Cks1-dependent sites cannot be primed by the CDK1 complexes tested and are likely to be primed by other kinases or else mediated by phosphorylation-independent docking interactions. Interestingly, these experiments, which were carried in biological duplicate separately from those shown in Figure 3E, also show that Cks1-dependent sites are depleted of the +1P and are instead enriched for a +3K (Figure 4J).

Taken together, our results here have shown that a subset of CDK1 phosphorylation sites lack the +1P consensus and that phosphorylation of these non-proline-directed sites by BCC is enhanced by the phosphoadaptor protein, Cks1. *In vitro*, Cks1-dependent phosphorylation is, in most cases, primed by CDK1 itself and promotes the multisite substrate phosphorylation.

Cks1- and Cyclin A-dependent phosphorylation sites are cell-cycle regulated

A crucial question is whether CDK1 phosphorylation observed *in vitro* is observed in living cells. The primary function of CDK activity is to drive cell-cycle progression via ordered phosphorylation of substrates, leading to increasing phosphorylation occupancy across the cell cycle with maximal occupancies observed in mitosis.¹ Therefore, we hypothesized that if *in vitro* sites are physiologically relevant, they should also be cell-cycle regulated (CCR) *in vivo*. We designed an experiment where cells enriched in different cell-cycle stages were directly compared against fixed cells phosphorylated *in vitro* by CDK1 (Figure 5A). These samples were analyzed together in a single quantitative TMT phosphoproteomics batch, which minimizes missing values. This internally controlled, relative quantitation approach enables

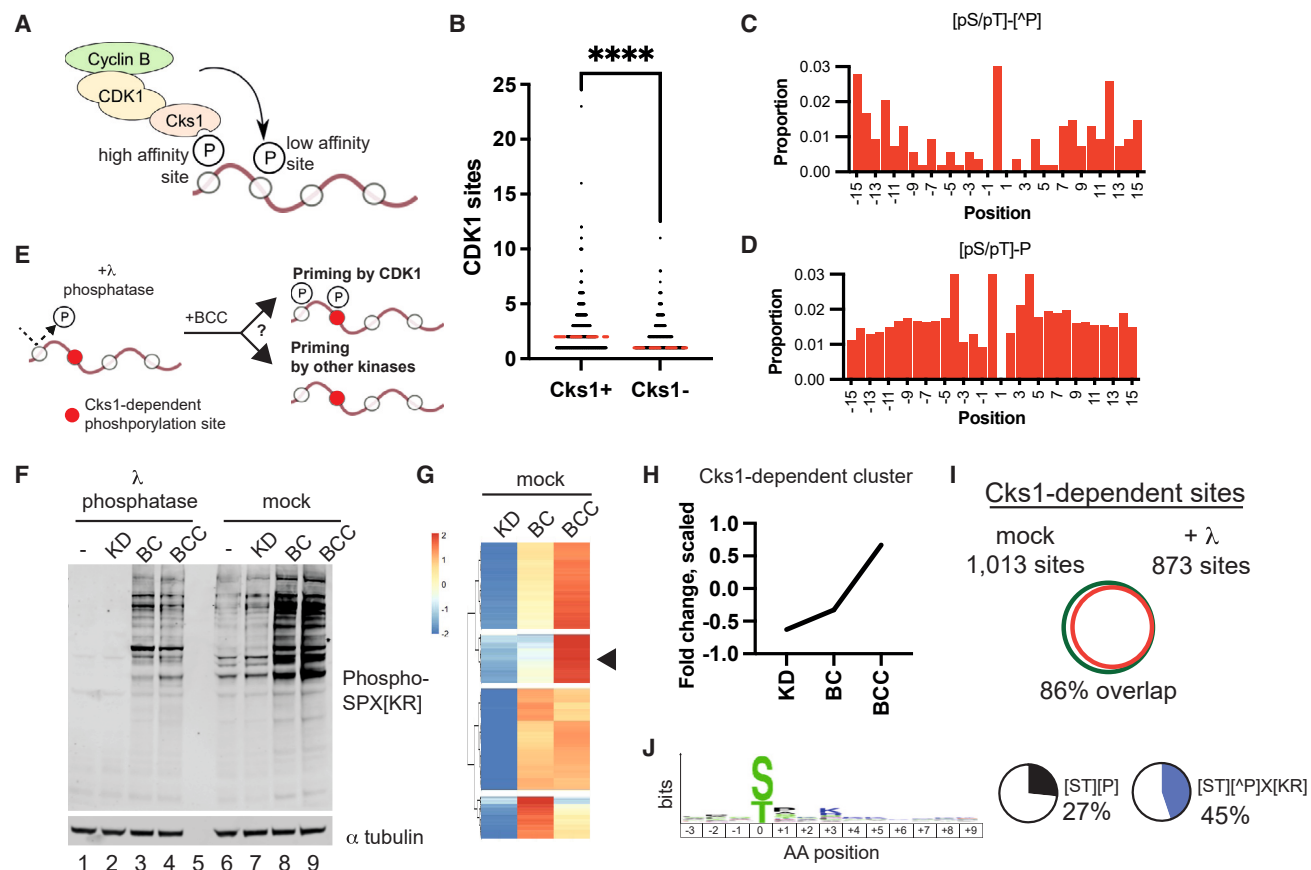


Figure 4. Cks1 promotes multisite phosphorylation of CDK1 substrates

(A) Model for Cks1 function in CDK1 substrate phosphorylation.
 (B) Dot plot representing the number of sites (y axis) phosphorylated on each protein substrate (dot). Only proteins unique to each cluster are shown. ****p < 0.0001 from a Student's t test; dotted lines represent the median.
 (C and D) The frequency of additional phosphorylation sites detected by phosphoproteomics within 15 residues of the phosphoacceptor for Cks1-dependent sites lacking the +1P (C) and CDK1 sites with a +1P (D).
 (E) Experimental design to investigate priming kinases for Cks1.
 (F) Western blot with anti-phospho-SPX[KR] motif antibody of lysates from fixed cells phosphorylated *in vitro* pre-treated either with λ phosphatase or mock. This antibody crossreacts with phosphorylated MAPK motifs, i.e., PXPSP.
 (G and H) Heatmap and line graph showing the identification of Cks1-dependent phosphorylation sites in mock-treated cells.
 (I) Overlap between sites that show Cks1 dependence in mock- versus λ phosphatase-treated cells.
 (J) Motif enrichment analysis of overlapping sites. Pie charts show the proportions of sites in the cluster with the indicated motif, e.g., +1P (black) or [ST][P]X[KR] (blue), where 'P' denotes any amino acid besides proline and X is any amino acid. Reproducible sites from two biological repeats are shown.

straightforward and comprehensive comparison between *in vitro* and *in vivo* phosphorylation.

G1- and G2/M populations were collected using centrifugal elutriation (Figure S4A). 9% of cells in the G2/M-enriched fraction were mitotic, judging by histone H3 S10 phosphorylation (H3pS10). In parallel, cells were arrested in prometaphase using STLC. Fixed G1- and G2/M-enriched cells were subjected to kinase assays using AC, BC, BCC, and KD, as above. 23,911 sites were detected in total (Tables S5 and S6), representing 5,242 protein substrates. 1,514 sites showed 2-fold or more phosphorylation in the G2/M-enriched sample compared with G1 cells. These sites were deemed interphase CCR (Figure 5A). Similarly, 4,198 sites showed 2-fold or more phosphorylation in STLC-arrested cells compared with the G2/M population and deemed to

be mitotic CCR (Figure 5A). In total, there were 5,102 sites either mitotic or interphase CCR. 6,924 sites showed 2-fold or more phosphorylation *in vitro* after incubation with one of the three active CDK1 complexes compared with samples treated with KD. Of these, 3,912 sites overlapped with either interphase or mitotic CCR sites (Figure 5B). SPX[KR] phosphorylation in STLC-arrested mitotic cells is more intense than G2/M-enriched cells subjected to phosphorylation by CDK1 *in vitro*, demonstrating that the phosphorylation occupancy achieved *in vitro* is at levels below the maximum achieved in cells arrested in mitosis (Figure S4B). These data demonstrate the fixed cell kinase assays phosphorylate sites to physiologically relevant levels and that a majority of *in vitro* CDK1 sites (56%) are phosphorylated in a CCR manner.

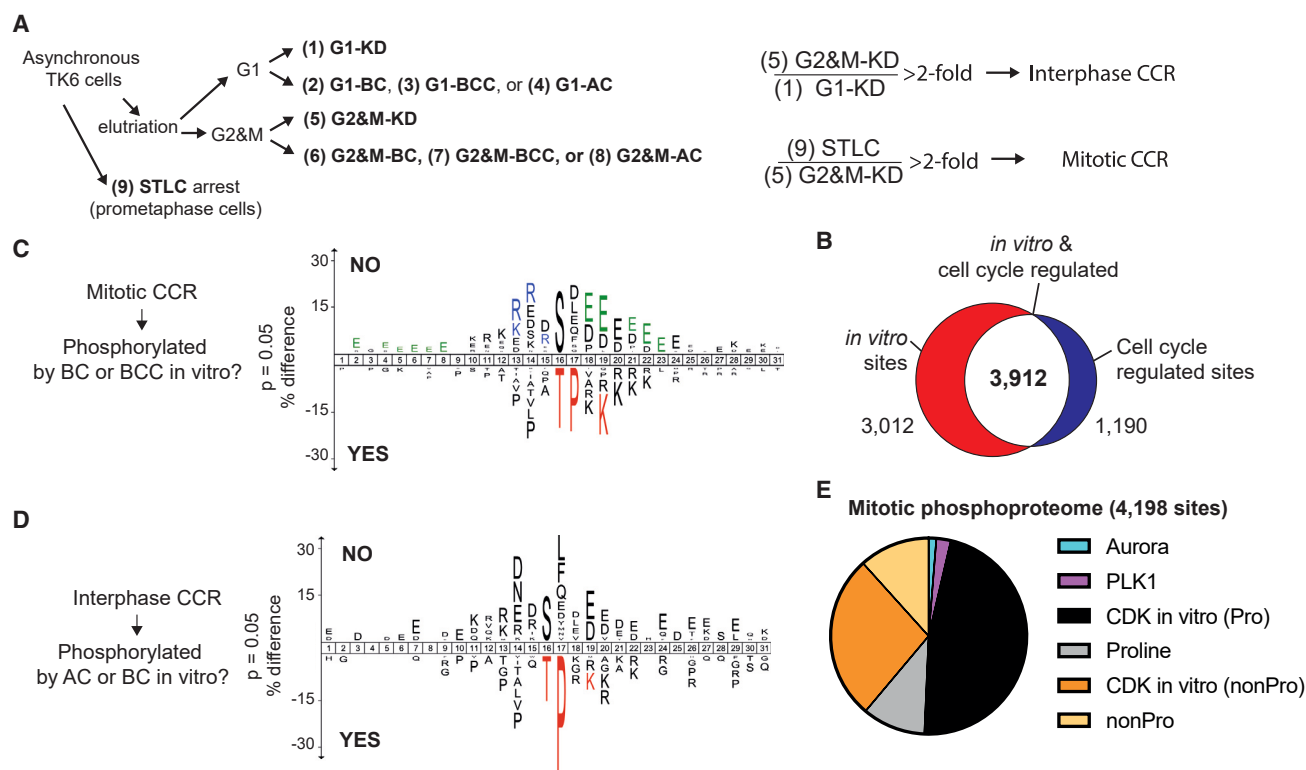


Figure 5. Non-proline-directed CDK phosphorylation sites *in vitro* are cell-cycle regulated in viable cells

(A) Design of experiment to identify both cell-cycle-regulated phosphorylation sites and *in vitro* CDK phosphorylated sites. All samples were combined into a single TMT analysis to minimize missing values.

(B) Overlap between sites phosphorylated *in vitro* by AC, BC, or BCC and the cell-cycle-regulated phosphoproteome.

(C) Enriched motifs for mitotic CCR sites that were either not phosphorylated by CDK1 *in vitro* (top) or phosphorylated by CDK1 *in vitro* (bottom).

(D) Motif enrichment analysis of interphase CCR sites that did not overlap with CDK1 *in vitro* targets (top) compared with that of those that overlapped (bottom).

(E) The proportion of phosphorylation sites in the mitotic regulated phosphoproteome that can be explained by consensus and direct CDK1 phosphorylation *in vitro*.

Sequence analysis of mitotic CCR sites not phosphorylated by CDK1 *in vitro* show a significant enrichment in motifs consistent with Aurora A/B and acidophilic kinases, including Polo-like kinases (Plk) 1/2/3 and casein kinase 2 (CK2) (Figure 5C, top). Interphase CCR sites not phosphorylated by CDK1 *in vitro* show enrichment in acidophilic kinases but no enrichment of Aurora A/B motifs. Non-CDK1 interphase CCR sites have a prominent enrichment of an acidic residue in the -2 position, consistent with a relaxed Plk1 consensus motif (Figure 5D, top). Both interphase and mitotic sites phosphorylated by CDK1 *in vitro* show an enrichment of the classic CDK consensus sequence (Figures 5C and 5D, bottom), which is virtually identical to a similar analysis of all *in vitro* CDK1 sites, including non-CCR sites (Figure 1C).

Next, we asked whether non-proline-directed sites phosphorylated by CDK1 *in vitro* are CCR in living cells (Figure 5E). Of the 4,198 mitotic CCR sites, 2,413 sites (57%) met a +1P minimum CDK consensus. Of these +1P CCR sites, 1,975 (82%) were phosphorylated by CDK1 *in vitro*. Only 100 and 53 of the mitotic CCR sites meet the strict consensus motifs for Plk1 and Aurora kinases ([KR][KR]X[ST]), respectively. The remaining 1,632 non-proline-directed mitotic CCR sites, which do not meet any of

the motifs described above, constituted 39% of the total mitotic CCR phosphoproteome. Strikingly, 1,142 of these non-proline-directed mitotic CCR sites, representing 70% of phosphorylation sites with no predicted upstream cell-cycle kinase, are phosphorylated by CDK1 *in vitro*. We therefore conclude that the majority of non-proline-directed mitotic CCR phosphorylation sites can be directly phosphorylated by CDK1. Taken together, our data show that 3,117 out of 4,198, or 74%, of the mitotic CCR phosphoproteome can be phosphorylated directly by CDK1 (proline and non-proline directed) (Figure 5E).

We then examined if there is evidence that Cks1-enhanced and Cyclin A-dependent phosphorylation sites are CCR. Indeed, Cks1-enhanced sites *in vitro* (Table S5) constitute 12.6% of the mitotic CCR phosphoproteome, of which 58% are non-proline directed. These Cks1-dependent, mitotic CCR sites show depletion of a +1P (Figure S4C). We reasoned that because AC is degraded during an extended prometaphase arrest (Figure S4B), AC-dependent sites will be subject to attrition in the STLC-arrested sample. CDK1 can phosphorylate substrates of interphase CDKs (CDK2/4/6). Therefore, to test if Cyclin A-dependent phosphorylation sites are also CCR, we performed the fixed cell kinase assay on interphase cells. G1 cells were

phosphorylated with either BC or AC *in vitro*. Hierarchical clustering identified a group of sites that were phosphorylated *in vitro* in a Cyclin A-dependent manner (Table S6). These sites represented 9% of the interphase CCR sites, and 47% of these sites matched the [ST][P]X[KR] motif. Sequence motif analysis of Cyclin A-dependent, interphase CCR sites show a depletion of a +1P and an enrichment of a +3K (Figure S4D).

A [ST][P]X[KR] sequence motif is enriched among non-proline-directed CDK1 sites

Our data show that both Cks1 and Cyclin A increase the frequency of non-proline-directed sites. Unlike Cyclin A, Cks1 is not targeted for degradation by APC/C-Cdc20 in early prometaphase and is found in cells in complex with Cyclin B-CDK1. Interestingly, a pool of Cyclin B-CDK1 is localized to the kinetochore corona and plays a role in spindle assembly checkpoint signaling.⁵⁷ We wondered if there was overlap between Cks1- and Cyclin A-dependent sites because phosphorylation of these sites could be “handed over” from Cyclin A-CDK1 (with or without Cks1) to Cyclin B-CDK1-Cks1 during prometaphase following Cyclin A degradation. The overlap between sites reproducibly dependent on Cyclin A (red, $n = 2$) and Cks1 (blue, $n = 2$) is shown in Figure 6A (Table S7). 44 sites on 41 proteins were in common. These included sites on Ki-67, MCAK (KIF2C), and Hec1 (NDC80), which all have functions in regulating chromosome segregation. The [ST][P]X[KR] motif that was observed individually for Cks1- and Cyclin A-dependent sites is strongly enriched in these overlapping sites (Figure 6B) and found in 39 out of the 44 sites.

We hypothesized that [ST][P]X[KR] CDK1 sites would be more susceptible to dephosphorylation by protein phosphatases active during prometaphase. This is because PP2A phosphatases show a preference for basic residues C-terminal to the phosphorylated site,⁵⁸ unlike +1P sites, which are disfavored by PP2A:B56.^{58–60} To test this hypothesis, we analyzed a dataset by Holder et al. in which mitotic cells were forced into anaphase by the addition of the Mps1 inhibitor AZ-3146 (Mps1i) and dephosphorylation was measured proteome-wide by phosphoproteomics.⁵⁸ The mean half-life ($t_{1/2}$) of [ST][P]X[KR] sites is ~ 17 min, which is significantly shorter than proline-directed sites and non-proline-directed sites in general, which both have an average $t_{1/2}$ of ~ 28 min (Figure 6C).

We next tested if enhancement of [ST][P]X[KR] phosphorylation by AC and BCC could be confirmed using purified protein substrates. Non-proline-directed +3K phosphorylation sites were detected on NDC80 (S76), PML (T473), and CDK7 (T25) (Table S7). NDC80 and PML show strong phosphorylation by CDK1 (Figures S5A and S5B). Interestingly, PML is hyperphosphorylated by BCC, but not by BC or AC (Figure S5A), consistent with a role for Cks1 in multisite phosphorylation. CDK7, on the other hand, shows no increase in its total phosphorylation signal over the no-kinase sample following treatment with any of the three CDK1 complexes tested (Figure S5C). Analysis of these reactions by MS, however, revealed site-specific sensitivity to CDK1. Phosphorylation of the [SP][P]X[KR] sites on all three substrates were enhanced by AC and BCC compared with BC (Figure 6D). This was not due to a difference in CDK1 activity because proline-directed sites on NDC80 and PML were phos-

phorylated to similar extents by all three CDK1 complexes tested (Figure 6E). Furthermore, the phosphorylation signal of the MAT1 subunit in CDK7 complex was more pronounced after incubation with AC compared with the other complexes (Figure S5C). In contrast, the overall phosphorylation of NDC80 was enhanced in the presence of Cks1 (Figure S5B). These results highlight the importance of site-specific detection by MS (Figures 6D and 6E), which can show differences from the total phosphorylation (Figure S5).

DISCUSSION

Many CCR phosphorylations do not meet the reported consensus sequences for cell-cycle kinases, indicating a major gap in our understanding. What are the missing kinases? The results presented suggest a surprising answer: CDK1. In this study, we showed that CDK1 can phosphorylate sites that do not match the classic CDK1 consensus sequence. Furthermore, this non-canonical CDK1 phosphorylation is widespread across the CCR phosphoproteome and is regulated by CDK1 subunit composition.

Using an internally controlled, quantitative phosphoproteomics approach, we demonstrated the majority of the mitotic CCR phosphoproteome (74%, out of 4,198 sites quantitated) can be directly phosphorylated by CDK1 *in vitro*. To what extent these sites are targets of direct CDK1 phosphorylation in cells is unknown. Even if a fraction of these sites are phosphorylated *in vivo* by other kinases, our data suggest that CDK1 can compensate, or complement, the activity of these kinases to phosphorylate these sites in mitosis. Phosphorylation handover from mTOR kinase to CDK1 has been recently described to suppress autophagy in mitosis by targeting the same proline-directed sites in ATG13, ULK1, and ATG14.⁶¹ Our data suggest that this handover is likely not limited to mTOR and other proline-directed kinases and likely extends to non-proline-directed kinases. To what extent this handover occurs and how this is regulated are open questions that will be important to address.

Cyclin-CDK complexes display different subcellular localizations *in vivo*.^{27,28} In fixed cells, cyclin-CDK complexes have equal access to cellular substrates (Figure S1G). Despite this, substrate proteins preferentially phosphorylated by AC differ in annotated functions and subcellular localization from BC. We observed no significant difference in RXL motifs between Cyclin A- and Cyclin B-dependent substrates, suggesting that there are additional sequence elements within substrate proteins encoding for specificity. Because subcellular organization and protein-protein interactions can be fixed in place with formaldehyde, it is possible that substrate choice in these assays is determined by interactions *in trans* instead of *cis* (i.e., within the same protein sequence as the phosphoacceptor residue). For example, high-affinity or high-avidity interactions between CDK1 complexes with a scaffolding protein could promote phosphorylation of other substrates proximal in space. Spatial determinants of substrate phosphorylation are key, for example, in models for the regulation of kinetochore-microtubule attachments by kinases like Aurora B and Plk1.^{62,63}

The fixed cell assays we have developed to understand CDK1 regulation can be extended to other cellular enzymes that produce a protein mass modification measurable by MS, e.g., ubiquitination. In contrast to *in vitro* assays on cell lysates, it is

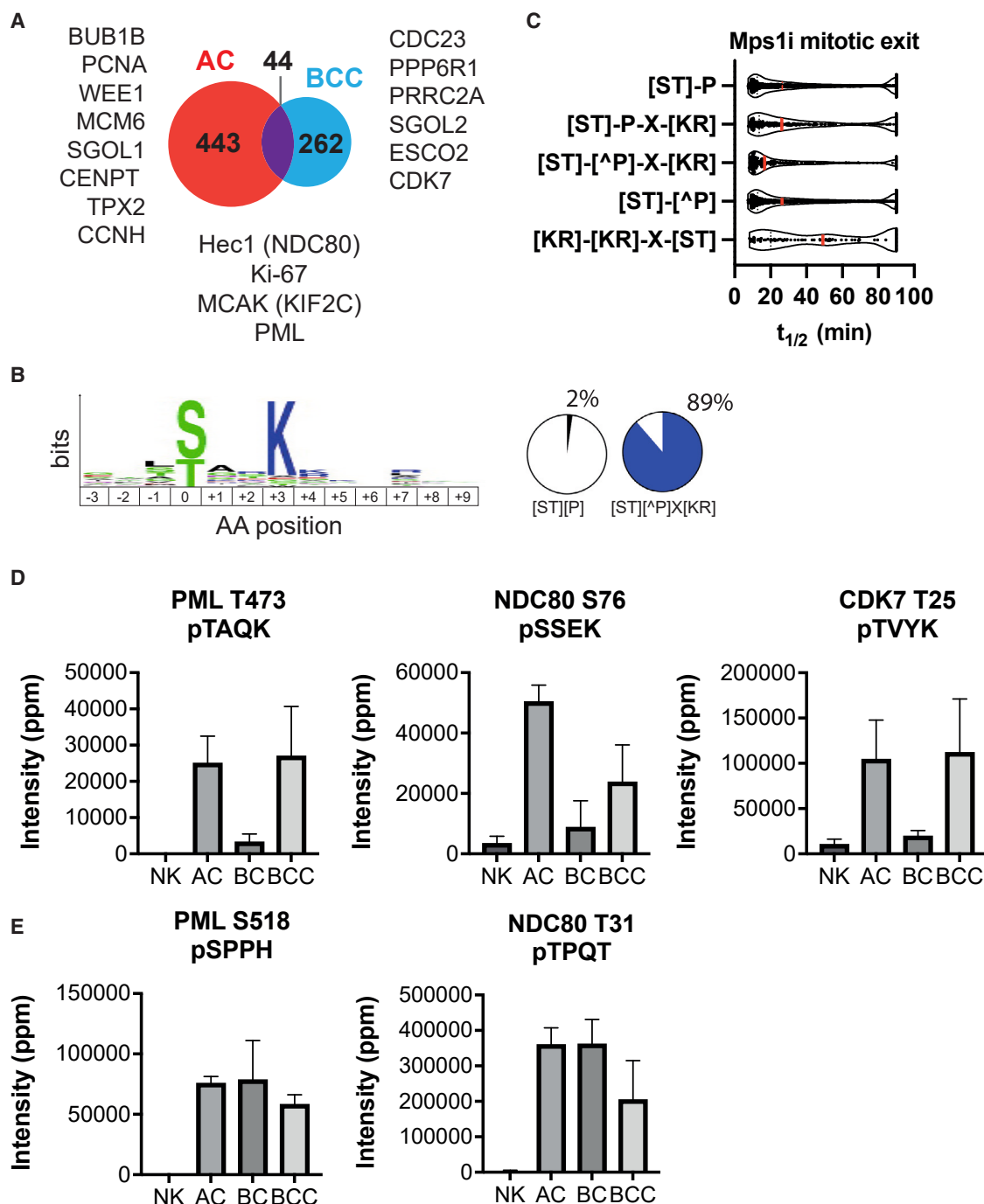


Figure 6. A non-proline-directed CDK consensus motif

(A) Overlap between sites reproducibly dependent on Cyclin A (red, N = 2) and Cks1 (blue, N = 2). Phosphorylation is reproducibly enhanced by Cks1 or Cyclin A (compared with Cyclin B-CDK1) for 44 sites (in purple). Selected substrate proteins that are shown for each.

(B) Motif enrichment analysis of sites in the overlap (purple shaded area) of (A).

(C) Dephosphorylation half-lives for phosphorylation sites detected in Holder et al.⁵⁸ matching the indicated sequence motifs, including proline-directed motifs ([ST]-P, [ST]-P-X-[KR]), the non-proline-directed CDK motif identified in (B) ([ST]-[[^]P]-X-[KR]), sites lacking a +1P ([ST]-[[^]P]), and sites matching the Aurora consensus ([KR]-[KR]-X-[ST]).

(D) Normalized intensities for phosphorylated [ST][[^]P]X[KR] sites on purified, recombinant PML, NDC80^{Broccoli}, and CDK7 subjected to *in vitro* kinase reactions with CDK1 complexes.

(E) Normalized intensities for phosphorylated proline-directed sites on the same substrates as (D).

straightforward to perform sequential enzymatic reactions on fixed cells (Figure 4). Sequential reactions can be used to study crosstalk between protein post-translational modifications in a highly controlled manner that is challenging in living cells with active negative and positive feedback mechanisms. We anticipate that the assay can be further improved by testing additional fixation and permeabilization reagents, including mild detergents to minimize disruption to protein tertiary structure.

Non-proline-directed CDK1 phosphorylation has been previously reported.^{37,64} Recently, it was shown that ~30% of direct CDK1 phosphorylation sites were non-proline directed in mESCs.³⁷ Interestingly, these sites showed an enrichment for a C-terminal basic residue, consistent with previous reports on individual substrates and the +3K motif described in our study.³⁸ We speculate these sites are especially important for spatial and temporal regulation in mitosis because they likely require high-avidity interactions for phosphorylation and are exquisitely sensitive to dephosphorylation (Figure 6C), thereby providing a wide dynamic range for rapidly tuning protein function.

In this study, we show that the qualitative nature of the CDK1 complex, namely the subunit composition, has a striking effect on the phosphorylation consensus sequence. In living cells, Cyclin A is targeted for destruction in prometaphase prior to Cyclin B destruction at anaphase onset.^{65,66} Thus, our data provide evidence for a regulated consensus sequence switch. CDK1/2 substrates are phosphorylated in both interphase and in mitotic cells but on distinct sites that have differential impact on protein function. Proteins in the Mcm family (Mcm1–7), which form the replicative helicase on chromatin to support DNA replication, are excellent examples of this. *Xenopus laevis* Mcm4 (x/Mcm4) is hyperphosphorylated in mitosis when replicative helicases are inactive. Complete dephosphorylation of x/Mcm4 prevents chromatin binding, whereas pre-replicative complexes bound to chromatin are hypo-phosphorylated, i.e., showing an intermediate level of phosphorylation between dephosphorylated and hyperphosphorylated.⁶⁷ In our analysis, two Mcm4 sites are detected, T23 and S120, which show high and low sensitivity to CDK1 phosphorylation *in vitro*. Interestingly, S120 meets the [ST][P]X[KR] consensus sequence for non-proline-directed CDK1 phosphorylation and is highly phosphorylated in mitosis (~84% stoichiometry).⁴⁰

Limitations of the study

The main limitation is that most of the findings are from formaldehyde-fixed cells. While this creates a simplified system that can be used to answer specific questions, like how non-catalytic subunits of CDK1 impact substrate choice, the system does not recapitulate the dynamic phosphorylation (and dephosphorylation) occurring in living cells nor the crowded macromolecular environment within cells that impact biochemical reaction kinetics. Using this simplified system, we found evidence for kinase phosphorylation consensus site switching that is dependent on CDK1 complex composition. It will now be important to investigate if the consensus site switching is observed in living cells and the functions of non-proline-directed CDK1 phosphorylation. Additionally, the structural and mechanistic basis for consensus site switching remains unclear and needs further investigation.

STAR★METHODS

Detailed methods are provided in the online version of this paper and include the following:

- **KEY RESOURCES TABLE**
- **RESOURCE AVAILABILITY**
 - Lead contact
 - Materials availability
 - Data and code availability
- **EXPERIMENTAL MODEL AND SUBJECT DETAILS**
- **METHOD DETAILS**
 - Cell culture and centrifugal elutriation
 - Protein expression and purification
 - In vitro kinase assays on fixed cells
 - Sample preparation for TMT phosphoproteomic analysis of fixed cells
 - Proteomics data analysis
 - *In vitro* kinase assays on recombinant proteins
- **QUANTIFICATION AND STATISTICAL ANALYSIS**

SUPPLEMENTAL INFORMATION

Supplemental information can be found online at <https://doi.org/10.1016/j.celrep.2023.112139>.

ACKNOWLEDGMENTS

We thank members of the Ly, JP Arulanandam, Julie Welburn, Constance Albert, Julian Blow, and Bill Earnshaw groups for helpful discussions. We thank the following for sharing reagents: Maria Alba Abad and JP Arulanandam (NDC80^{Broccoli}) and Ania Eugui Anta, Anna Plechanovova, and Ron Hay (PML). We thank the FingerPrints Proteomics Facility, Shaun Webb (Wellcome Center for Cell Biology Bioinformatics Core), and the Edinburgh Protein Production Facility for technical support and advice. This work is supported by a Wellcome Trust and Royal Society Sir Henry Dale Fellowship to T.L. (206211/Z/17/Z); a Darwin Trust PhD studentship to A.a.-R.; a UK Medical Research Council Program Grant to J.A.E. (MR/N009738/1); core funding for the Wellcome Centre for Cell Biology (091020); a Wellcome Multi-User Equipment Grant to T.L. (218305/Z/19/Z); and a Wellcome Innovation Award for MS equipment (218448/Z/19/Z).

AUTHOR CONTRIBUTIONS

Conceptualization, T.L.; supervision, T.L. and J.A.E.; formal analysis, T.L., A.a.-R., E.K., and J.A.E.; writing – original draft, T.L. and A.a.-R.; funding acquisition, T.L. and J.A.E.; investigation, T.L., A.a.-R., and E.K.; writing – review & editing, T.L., A.a.-R., and S.K.; methodology, A.a.-R. and S.K.; resources, S.K.

DECLARATION OF INTERESTS

The authors declare no competing interests.

Received: June 6, 2022

Revised: November 17, 2022

Accepted: February 2, 2023

REFERENCES

1. Swaffer, M.P., Jones, A.W., Flynn, H.R., Snijders, A.P., and Nurse, P. (2016). CDK substrate phosphorylation and ordering the cell cycle. *Cell* 167, 1750–1761.e16. <https://doi.org/10.1016/j.cell.2016.11.034>.

2. Morgan, D.O. (1997). CYCLIN-DEPENDENT KINASES: engines, clocks, and microprocessors. *Annu. Rev. Cell Dev. Biol.* 13, 261–291. <https://doi.org/10.1146/annurev.cellbio.13.1.261>.
3. Gavet, O., and Pines, J. (2010). Progressive activation of CyclinB1-cdk1 coordinates entry to mitosis. *Dev. Cell* 18, 533–543. <https://doi.org/10.1016/j.devcel.2010.02.013>.
4. Santamaría, D., Barrière, C., Cerqueira, A., Hunt, S., Tardy, C., Newton, K., Cáceres, J.F., Dubus, P., Malumbres, M., and Barbacid, M. (2007). Cdk1 is sufficient to drive the mammalian cell cycle. *Nature* 448, 811–815. <https://doi.org/10.1038/nature06046>.
5. Coudreuse, D., and Nurse, P. (2010). Driving the cell cycle with a minimal CDK control network. *Nature* 468, 1074–1079. <https://doi.org/10.1038/nature09543>.
6. Satyanarayanan, A., and Kaldis, P. (2009). Mammalian cell-cycle regulation: several Cdk, numerous cyclins and diverse compensatory mechanisms. *Oncogene* 28, 2925–2939. <https://doi.org/10.1038/onc.2009.170>.
7. Mitra, J., and Enders, G.H. (2004). Cyclin A/Cdk2 complexes regulate activation of Cdk1 and Cdc25 phosphatases in human cells. *Oncogene* 23, 3361–3367. <https://doi.org/10.1038/sj.onc.1207446>.
8. Russell, P., and Nurse, P. (1986). cdc25+ functions as an inducer in the mitotic control of fission yeast. *Cell* 45, 145–153. [https://doi.org/10.1016/0092-8674\(86\)90546-5](https://doi.org/10.1016/0092-8674(86)90546-5).
9. Russell, P., and Nurse, P. (1987). Negative regulation of mitosis by wee1+, a gene encoding a protein kinase homolog. *Cell* 49, 559–567. [https://doi.org/10.1016/0092-8674\(87\)90458-2](https://doi.org/10.1016/0092-8674(87)90458-2).
10. Hégarat, N., Crncec, A., Suarez Peredo Rodriguez, M.F., Echegaray Iturra, F., Gu, Y., Busby, O., Lang, P.F., Barr, A.R., Bakal, C., Kanemaki, M.T., et al. (2020). Cyclin A triggers Mitosis either via the Greatwall kinase pathway or Cyclin B. *EMBO J.* 39, e104419. <https://doi.org/10.15252/emboj.2020104419>.
11. Lau, H.W., Ma, H.T., Yeung, T.K., Tam, M.Y., Zheng, D., Chu, S.K., and Poon, R.Y.C. (2021). Quantitative differences between cyclin-dependent kinases underlie the unique functions of CDK1 in human cells. *Cell Rep.* 37, 109808. <https://doi.org/10.1016/j.celrep.2021.109808>.
12. McGrath, D.A., Balog, E.R.M., Köivomägi, M., Lucena, R., Mai, M.V., Hirschi, A., Kellogg, D.R., Loog, M., and Rubin, S.M. (2013). Cks confers specificity to phosphorylation-dependent CDK signaling pathways. *Nat. Struct. Mol. Biol.* 20, 1407–1414. <https://doi.org/10.1038/nsmb.2707>.
13. Martinsson-Ahlzén, H.S., Liberal, V., Grünenfelder, B., Chaves, S.R., Spruck, C.H., and Reed, S.I. (2008). Cyclin-dependent kinase-associated proteins Cks1 and Cks2 are essential during early embryogenesis and for cell cycle progression in somatic cells. *Mol. Cell Biol.* 28, 5698–5709. <https://doi.org/10.1128/mcb.01833-07>.
14. Ganoh, D., Bornstein, G., Ko, T.K., Larsen, B., Tyers, M., Pagano, M., and Hershko, A. (2001). The cell-cycle regulatory protein Cks1 is required for SCFSkp2-mediated ubiquitinylation of p27. *Nat. Cell Biol.* 3, 321–324. <https://doi.org/10.1038/35060126>.
15. Sitry, D., Seeliger, M.A., Ko, T.K., Ganoh, D., Breward, S.E., Itzhaki, L.S., Pagano, M., and Hershko, A. (2002). Three different binding sites of Cks1 are required for p27-ubiquitin ligation. *J. Biol. Chem.* 277, 42233–42240. <https://doi.org/10.1074/jbc.M205254200>.
16. Köivomägi, M., Valk, E., Venta, R., Iofik, A., Lepiku, M., Balog, E.R.M., Rubin, S.M., Morgan, D.O., and Loog, M. (2011). Cascades of multisite phosphorylation control Sic1 destruction at the onset of S phase. *Nature* 480, 128–131. <https://doi.org/10.1038/nature10560>.
17. Köivomägi, M., Örd, M., Iofik, A., Valk, E., Venta, R., Faustova, I., Kivi, R., Balog, E.R.M., Rubin, S.M., and Loog, M. (2013). Multisite phosphorylation networks as signal processors for Cdk1. *Nat. Struct. Mol. Biol.* 20, 1415–1424. <https://doi.org/10.1038/nsmb.2706>.
18. Fisher, D.L., and Nurse, P. (1996). A single fission yeast mitotic cyclin B p34cdc2 kinase promotes both S-phase and mitosis in the absence of G1 cyclins. *EMBO J.* 15, 850–860.
19. Stern, B., and Nurse, P. (1996). A quantitative model for the cdc2 control of S phase and mitosis in fission yeast. *Trends Genet.* 12, 345–350. [https://doi.org/10.1016/S0168-9525\(96\)80016-3](https://doi.org/10.1016/S0168-9525(96)80016-3).
20. Loog, M., and Morgan, D.O. (2005). Cyclin specificity in the phosphorylation of cyclin-dependent kinase substrates. *Nature* 434, 104–108. <https://doi.org/10.1038/nature03329>.
21. Örd, M., and Loog, M. (2019). How the cell cycle clock ticks. *Mol. Biol. Cell* 30, 169–172. <https://doi.org/10.1091/mbc.E18-05-0272>.
22. Örd, M., Venta, R., Möll, K., Valk, E., and Loog, M. (2019). Cyclin-specific docking mechanisms reveal the complexity of M-CDK function in the cell cycle. *Mol. Cell* 75, 76–89.e3. <https://doi.org/10.1016/j.molcel.2019.04.026>.
23. Takeda, D.Y., Wohlschlegel, J.A., and Dutta, A. (2001). A bipartite substrate recognition motif for cyclin-dependent kinases. *J. Biol. Chem.* 276, 1993–1997. <https://doi.org/10.1074/jbc.M005719200>.
24. Adams, P.D., Sellers, W.R., Sharma, S.K., Wu, A.D., Nalin, C.M., and Kaelin, W.G. (1996). Identification of a cyclin-cdk2 recognition motif present in substrates and p21-like cyclin-dependent kinase inhibitors. *Mol. Cell Biol.* 16, 6623–6633. <https://doi.org/10.1128/mcb.16.12.6623>.
25. Schulman, B.A., Lindstrom, D.L., and Harlow, E. (1998). Substrate recruitment to cyclin-dependent kinase 2 by a multipurpose docking site on cyclin A. *Proc. Natl. Acad. Sci. USA* 95, 10453–10458. <https://doi.org/10.1073/pnas.95.18.10453>.
26. Lowe, E.D., Tews, I., Cheng, K.Y., Brown, N.R., Gul, S., Noble, M.E.M., Gambin, S.J., and Johnson, L.N. (2002). Specificity determinants of recruitment peptides bound to phospho-CDK2/cyclin A. *Biochemistry* 41, 15625–15634. <https://doi.org/10.1021/bi0268910>.
27. Moore, J.D., Kornbluth, S., and Hunt, T. (2002). Identification of the nuclear localization signal in Xenopus cyclin E and analysis of its role in replication and mitosis. *Mol. Biol. Cell* 13, 4388–4400. <https://doi.org/10.1091/mbc.E02-07-0449>.
28. Jackman, M., Kubota, Y., Den Elzen, N., Hagting, A., and Pines, J. (2002). Cyclin A- and cyclin E-Cdk complexes shuttle between the nucleus and the cytoplasm. *Mol. Biol. Cell* 13, 1030–1045. <https://doi.org/10.1091/mbc.01-07-0361>.
29. Toyoshima, F., Moriguchi, T., Wada, A., Fukuda, M., and Nishida, E. (1998). Nuclear export of cyclin B1 and its possible role in the DNA damage-induced G2 checkpoint. *EMBO J.* 17, 2728–2735. <https://doi.org/10.1093/emboj/17.10.2728>.
30. Pagliuca, F.W., Collins, M.O., Lichawska, A., Zegerman, P., Choudhary, J.S., and Pines, J. (2011). Quantitative proteomics reveals the basis for the biochemical specificity of the cell-cycle machinery. *Mol. Cell* 43, 406–417. <https://doi.org/10.1016/j.molcel.2011.05.031>.
31. Gong, D., Pomeroy, J.R., Myers, J.W., Gustavsson, C., Jones, J.T., Hahn, A.T., Meyer, T., and Ferrell, J.E. (2007). Cyclin A2 regulates nuclear-envelope breakdown and the nuclear accumulation of cyclin B1. *Curr. Biol.* 17, 85–91. <https://doi.org/10.1016/j.cub.2006.11.066>.
32. Kabeche, L., and Compton, D.A. (2013). Cyclin A regulates microtubule microtubules to promote faithful chromosome segregation. *Nature* 502, 110–113. <https://doi.org/10.1038/nature12507>.
33. Trunnell, N.B., Poon, A.C., Kim, S.Y., and Ferrell, J.E., Jr. (2011). Ultrasensitivity in the regulation of Cdc25C by Cdk1. *Mol. Cell* 41, 263–274. <https://doi.org/10.1016/j.molcel.2011.01.012>.
34. Brown, N.R., Korolchuk, S., Martin, M.P., Stanley, W.A., Moukhametzianov, R., Noble, M.E.M., and Endicott, J.A. (2015). CDK1 structures reveal conserved and unique features of the essential cell cycle CDK. *Nat. Commun.* 6, 6769. <https://doi.org/10.1038/ncomms7769>.
35. Brown, N.R., Noble, M.E., Endicott, J.A., and Johnson, L.N. (1999). The structural basis for specificity of substrate and recruitment peptides for cyclin-dependent kinases. *Nat. Cell Biol.* 1, 438–443. <https://doi.org/10.1038/15674>.
36. Mok, J., Kim, P.M., Lam, H.Y.K., Piccirillo, S., Zhou, X., Jeschke, G.R., Sheridan, D.L., Parker, S.A., Desai, V., Jwa, M., et al. (2010). Deciphering

- protein kinase specificity through large-scale analysis of yeast phosphorylation site motifs. *Sci. Signal.* 3, ra12. <https://doi.org/10.1126/scisignal.2000482>.
37. Michowski, W., Chick, J.M., Chu, C., Kolodziejczyk, A., Wang, Y., Suski, J.M., Abraham, B., Anders, L., Day, D., Dunkl, L.M., et al. (2020). Cdk1 controls global epigenetic landscape in embryonic stem cells. *Mol. Cell* 78, 459–476.e13. <https://doi.org/10.1016/j.molcel.2020.03.010>.
38. Suzuki, K., Sako, K., Akiyama, K., Isoda, M., Senoo, C., Nakajo, N., and Sagata, N. (2015). Identification of non-Ser/Thr-Pro consensus motifs for Cdk1 and their roles in mitotic regulation of C2H2 zinc finger proteins and Ect2. *Sci. Rep.* 5, 7929. <https://doi.org/10.1038/srep07929>.
39. Watson, N.A., Cartwright, T.N., Lawless, C., Cámara-Donoso, M., Sen, O., Sako, K., Hirota, T., Kimura, H., and Higgins, J.M.G. (2020). Kinase inhibition profiles as a tool to identify kinases for specific phosphorylation sites. *Nat. Commun.* 11, 1684. <https://doi.org/10.1038/s41467-020-15428-0>.
40. Olsen, J.V., Vermeulen, M., Santamaria, A., Kumar, C., Miller, M.L., Jensen, L.J., Gnad, F., Cox, J., Jensen, T.S., Nigg, E.A., et al. (2010). Quantitative Phosphoproteomics Reveals Widespread Full Phosphorylation Site Occupancy During Mitosis. *Sci. Signal* 3, ra3.
41. Dephoure, N., Zhou, C., Villén, J., Beausoleil, S.A., Bakalarski, C.E., Elledge, S.J., and Gygi, S.P. (2008). A quantitative atlas of mitotic phosphorylation. *Proc. Natl. Acad. Sci. USA* 105, 10762–10767. <https://doi.org/10.1073/pnas.0805139105>.
42. Herr, P., Boström, J., Rullman, E., Rudd, S.G., Vesterlund, M., Lehtö, J., Helleday, T., Maddalo, G., and Altun, M. (2020). Cell cycle profiling reveals protein oscillation, phosphorylation, and localization dynamics. *Mol. Cell. Proteomics* 19, 608–623. <https://doi.org/10.1074/mcp.RA120.001938>.
43. Ly, T., Whigham, A., Clarke, R., Brenes-Murillo, A.J., Estes, B., Madhesian, D., Lundberg, E., Wadsworth, P., and Lamond, A.I. (2017). Proteomic analysis of cell cycle progression in asynchronous cultures, including mitotic subphases, using PRIMMUS. *Elife* 6, e27574. <https://doi.org/10.7554/eLife.27574>.
44. Vigneron, S., Brioudes, E., Burgess, A., Labbé, J.C., Lorca, T., and Castro, A. (2009). Greatwall maintains mitosis through regulation of PP2A. *EMBO J.* 28, 2786–2793. <https://doi.org/10.1038/emboj.2009.228>.
45. Castilho, P.V., Williams, B.C., Mochida, S., Zhao, Y., and Goldberg, M.L. (2009). The M phase kinase Greatwall (Gwl) promotes inactivation of PP2A/B55delta, a phosphatase directed against CDK phosphosites. *Mol. Biol. Cell* 20, 4777–4789. <https://doi.org/10.1091/mbc.e09-07-0643>.
46. Kelly, V., al-Rawi, A., Lewis, D., Kustatscher, G., and Ly, T. (2022). Low cell number proteomic analysis using in-cell protease digests reveals a robust signature for cell cycle state classification. *Mol. Cell. Proteomics* 21, 100169. <https://doi.org/10.1016/j.mcpro.2021.100169>.
47. Kettenbach, A.N., Schweppe, D.K., Faherty, B.K., Pechenick, D., Pletnev, A.A., and Gerber, S.A. (2011). Quantitative phosphoproteomics identifies substrates and functional modules of Aurora and Polo-like kinase activities in mitotic cells. *Sci. Signal.* 4, rs5. <https://doi.org/10.1126/scisignal.2001497>.
48. Holt, L.J., Tuch, B.B., Villén, J., Johnson, A.D., Gygi, S.P., and Morgan, D.O. (2009). Global analysis of cdk1 substrate phosphorylation sites provides insights into evolution. *Science* 325, 1682–1686. <https://doi.org/10.1126/science.1172867>.
49. Ly, T., Ahmad, Y., Shlien, A., Soroka, D., Mills, A., Emanuele, M.J., Stratton, M.R., and Lamond, A.I. (2014). A proteomic chronology of gene expression through the cell cycle in human myeloid leukemia cells. *Elife* 3, e01630. <https://doi.org/10.7554/eLife.01630>.
50. Wiśniewski, J.R., Hein, M.Y., Cox, J., and Mann, M. (2014). A "proteomic ruler" for protein copy number and concentration estimation without spike-in standards. *Mol. Cell. Proteomics* 13, 3497–3506. <https://doi.org/10.1074/mcp.M113.037309>.
51. Gavet, O., and Pines, J. (2010). Activation of cyclin B1–Cdk1 synchronizes events in the nucleus and the cytoplasm at mitosis. *J. Cell Biol.* 189, 247–259. <https://doi.org/10.1083/jcb.200909144>.
52. Cundell, M.J., Hutter, L.H., Nunes Bastos, R., Poser, E., Holder, J., Mohammed, S., Novak, B., and Barr, F.A. (2016). A PP2A-B55 recognition signal controls substrate dephosphorylation kinetics during mitotic exit. *J. Cell Biol.* 214, 539–554. <https://doi.org/10.1083/jcb.201606033>.
53. Godfrey, M., Touati, S.A., Kataria, M., Jones, A., Snijders, A.P., and Uhlmann, F. (2017). PP2ACdc55 phosphatase imposes ordered cell-cycle phosphorylation by opposing threonine phosphorylation. *Mol. Cell* 65, 393–402.e3. <https://doi.org/10.1016/j.molcel.2016.12.018>.
54. Hein, J.B., Hertz, E.P.T., Garvanska, D.H., Kruse, T., and Nilsson, J. (2017). Distinct kinetics of serine and threonine dephosphorylation are essential for mitosis. *Nat. Cell Biol.* 19, 1433–1440. <https://doi.org/10.1038/ncb3634>.
55. Krasinska, L., Domingo-Sananes, M.R., Kapuy, O., Parisi, N., Harker, B., Moorhead, G., Rossignol, M., Novák, B., Fisher, D., and Fisher, D. (2011). Protein phosphatase 2A controls the order and dynamics of cell-cycle transitions. *Mol. Cell* 44, 437–450. <https://doi.org/10.1016/j.molcel.2011.10.007>.
56. Mochida, S., Ikeo, S., Gannon, J., and Hunt, T. (2009). Regulated activity of PP2A-B55 delta is crucial for controlling entry into and exit from mitosis in *Xenopus* egg extracts. *EMBO J.* 28, 2777–2785. <https://doi.org/10.1038/emboj.2009.238>.
57. Allan, L.A., Camacho Reis, M., Ciossani, G., Huis in 't Veld, P.J., Wohlge-muth, S., Kops, G.J., Musacchio, A., and Saurin, A.T. (2020). Cyclin B1 scaffolds MAD 1 at the kinetochore corona to activate the mitotic checkpoint. *EMBO J.* 39, e103180. <https://doi.org/10.15252/emboj.2019103180>.
58. Holder, J., Mohammed, S., and Barr, F.A. (2020). Ordered dephosphorylation initiated by the selective proteolysis of cyclin B drives mitotic exit. *Elife* 9, e59885. <https://doi.org/10.7554/ELIFE.59885>.
59. Bancroft, J., Holder, J., Geraghty, Z., Alfonso-Pérez, T., Murphy, D., Barr, F.A., and Gruneberg, U. (2020). PP1 promotes cyclin B destruction and the metaphase-anaphase transition by dephosphorylating CDC20. *Mol. Biol. Cell* 31, 2315–2330. <https://doi.org/10.1091/mbc.E20-04-0252>.
60. Kruse, T., Gnosa, S.P., Nasa, I., Garvanska, D.H., Hein, J.B., Nguyen, H., Samsøe-Petersen, J., Lopez-Mendez, B., Hertz, E.P.T., Schwarz, J., et al. (2020). Mechanisms of site-specific dephosphorylation and kinase opposition imposed by PP2A regulatory subunits. *EMBO J.* 39, e103695. <https://doi.org/10.15252/emboj.2019103695>.
61. Odle, R.I., Florey, O., Ktistakis, N.T., and Cook, S.J. (2021). CDK1, the other 'master regulator' of autophagy. *Trends Cell Biol.* 31, 95–107.
62. Singh, P., Pesenti, M.E., Maffini, S., Carmignani, S., Hedtfeld, M., Petrovic, A., Srinivasamani, A., Bange, T., and Musacchio, A. (2021). BUB1 and CENP-U, primed by CDK1, are the main PLK1 kinetochore receptors in mitosis. *Mol. Cell* 81, 67–87.e9. <https://doi.org/10.1016/j.molcel.2020.10.040>.
63. Samejima, K., Platani, M., Wolny, M., Ogawa, H., Vargiu, G., Knight, P.J., Peckham, M., and Earnshaw, W.C. (2015). The inner centromere protein (INCENP) coil is a single α -helix (SAH) domain that binds directly to microtubules and is important for chromosome passenger complex (CPC) localization and function in mitosis. *J. Biol. Chem.* 290, 21460–21472. <https://doi.org/10.1074/jbc.M115.645317>.
64. Blethrow, J.D., Glavy, J.S., Morgan, D.O., and Shokat, K.M. (2008). Covalent capture of kinase-specific phosphopeptides reveals Cdk1-cyclin B substrates. *Proc. Natl. Acad. Sci. USA* 105, 1442–1447. <https://doi.org/10.1073/pnas.0708966105>.
65. Whitfield, W.G., Gonzalez, C., Maldonado-Codina, G., and Glover, D.M. (1990). The A- and B-type cyclins of *Drosophila* are accumulated and destroyed in temporally distinct events that define separable phases of the G2-M transition. *EMBO J.* 9, 2563–2572. <https://doi.org/10.1002/j.1460-2075.1990.tb07437.x>.
66. Hunt, T., Luca, F.C., and Ruderman, J.V. (1992). The requirements for protein synthesis and degradation, and the control of destruction of cyclins A and B in the meiotic and mitotic cell cycles of the clam embryo. *J. Cell Biol.* 116, 707–724. <https://doi.org/10.1083/jcb.116.3.707>.

67. Pereverzeva, I., Whitmire, E., Khan, B., and Coué, M. (2000). Distinct phosphoisoforms of the *Xenopus* Mcm4 protein regulate the function of the mcm complex. *Mol. Cell Biol.* 20, 3667–3676. <https://doi.org/10.1128/MCB.20.10.3667-3676.2000>.
68. Petri, E.T., Errico, A., Escobedo, L., Hunt, T., and Basavappa, R. (2007). The crystal structure of human cyclin B. *Cell Cycle* 6, 1342–1349. <https://doi.org/10.4161/cc.6.11.4297>.
69. Brown, N.R., Noble, M.E., Lawrie, A.M., Morris, M.C., Tunnah, P., Divita, G., Johnson, L.N., and Endicott, J.A. (1999). Effects of phosphorylation of threonine 160 on cyclin-dependent kinase 2 structure and activity. *J. Biol. Chem.* 274, 8746–8756. <https://doi.org/10.1074/jbc.274.13.8746>.
70. Brown, N.R., Noble, M.E., Endicott, J.A., Garman, E.F., Wakatsuki, S., Mitchell, E., Rasmussen, B., Hunt, T., and Johnson, L.N. (1995). The crystal structure of cyclin A. *Structure* 3, 1235–1247. [https://doi.org/10.1016/S0969-2126\(01\)00259-3](https://doi.org/10.1016/S0969-2126(01)00259-3).
71. Kucharski, T.J., Hards, R., Vandal, S.E., Abad, M.A., Jeyaparakash, A.A., Kaye, E., Al-Rawi, A., Ly, T., Godek, K.M., Gerber, S.A., and Compton, D.A. (2022). Small changes in phospho-occupancy at the kinetochore-microtubule interface drive mitotic fidelity. *J. Cell Biol.* 221, e202107107. <https://doi.org/10.1083/jcb.202107107>.
72. McAlister, G.C., Nusinow, D.P., Jedrychowski, M.P., Wühr, M., Huttlin, E.L., Erickson, B.K., Rad, R., Haas, W., and Gygi, S.P. (2014). MultiNotch MS3 enables accurate, sensitive, and multiplexed detection of differential expression across cancer cell line proteomes. *Anal. Chem.* 86, 7150–7158. <https://doi.org/10.1021/ac502040v>.
73. Cox, J., and Mann, M. (2008). MaxQuant enables high peptide identification rates, individualized p.p.b.-range mass accuracies and proteome-wide protein quantification. *Nat. Biotechnol.* 26, 1367–1372. <https://doi.org/10.1038/nbt.1511>.
74. Crooks, G.E., Hon, G., Chandonia, J.-M., and Brenner, S.E. (2004). WebLogo: a sequence logo generator. *Genome Res.* 14, 1188–1190. <https://doi.org/10.1101/gr.849004>.
75. Colaert, N., Helsens, K., Martens, L., Vandekerckhove, J., and Gevaert, K. (2009). Improved visualization of protein consensus sequences by ice-Logo. *Nat. Methods* 6, 786–787. <https://doi.org/10.1038/nmeth1109-786>.
76. Schmidt, J.C., Arthanari, H., Boeszoermyeni, A., Dashkevich, N.M., Wilson-Kubalek, E.M., Monnier, N., Markus, M., Oberer, M., Milligan, R.A., Bathe, M., et al. (2012). The kinetochore-bound Ska1 complex tracks depolymerizing microtubules and binds to curved protofilaments. *Dev. Cell* 23, 968–980. <https://doi.org/10.1016/j.devcel.2012.09.012>.
77. MacLean, B., Tomazela, D.M., Shulman, N., Chambers, M., Finney, G.L., Frewen, B., Kern, R., Tabb, D.L., Liebler, D.C., and MacCoss, M.J. (2010). Skyline: an open source document editor for creating and analyzing targeted proteomics experiments. *Bioinformatics* 26, 966–968. <https://doi.org/10.1093/bioinformatics/btq054>.

STAR★METHODS

KEY RESOURCES TABLE

REAGENT or RESOURCE	SOURCE	IDENTIFIER
Antibodies		
Rabbit anti- Phospho-SPX[KR] motif	Cell Signaling Technologies	2325S;RRID:AB_331820
Rabbit anti-human Cyclin A2	Abcam	ab32386;RRID:AB_2244193
Mouse anti-human GAPDH	Santa Cruz Biotechnology	sc-365062;RRID:AB_10847862
Mouse anti-human Alpha-Tubulin	Sigma-Aldrich	CP06-100UG;RRID:AB_2617116
Mouse anti-human H3pS10	Cell Signaling Technologies	29237S;RRID:AB_2798971
Bacterial and virus strains		
<i>E. coli</i> DH5 α	Invitrogen	18,265-017
<i>E. coli</i> Rosetta2 (DE3) pLYS-S	Novagen	709,564
Chemicals, peptides, and recombinant proteins		
Propidium Iodide (PI)	Sigma-Aldrich	P4864-10ML
Diamidino phenylindole (DAPI)	Sigma-Aldrich	D9542-10MG
S-trityl-L-Cysteine (STLC)	Sigma-Aldrich	164,739-5G
Adenosine triphosphate (ATP)	Sigma-Aldrich	A2383-5G
Tris carboxyethyl phosphine (TCEP)	Thermo-Fisher Scientific	PG82080
Iodoacetamide	Sigma-Aldrich	I1149-5G
Triethylammonium bicarbonate (TEAB)	Sigma-Aldrich	T7408-100ML
HIPPR detergent removal columns	Thermo-Fisher Scientific	88,305
Cyclin H-CDK7-MAT1	MRC-PPU	DU 49574
Tandem mass tag (TMTpro) 16 plex	Thermo-Fisher Scientific	A44520
Hydroxyl amine	Thermo-Fisher Scientific	90,115
Acetonitrile	Thermo-Fisher Scientific	A955-1
Methanol	Fisher Scientific	11,976,961
Formic acid	Thermo Fisher Scientific	28,905
Acetic acid	Thermo Fisher Scientific	A11350
Trifluoroacetic acid (TFA)	Sigma-Aldrich	302,031
ammonium hydroxide	Sigma-Aldrich	338,818-100ML
Ammonium formate	Sigma-Aldrich	78,314-100ML-F
Glycolic acid	Sigma-Aldrich	420,581-100ML
cOMplete protease inhibitor cocktail	Sigma-Aldrich	11,836,170,001
Phosphatase inhibitor cocktail (PhosSTOP)	Roche	4,906,837,001
λ Phosphatase		
Trypsin protease	Thermo-Fisher Scientific	90,058
Benzonase	EMD Millipore	70,664-10KUN
para-nitrophenylphosphate	NEB	P0757S
MagReSyn® Ti-IMAC	2BScientific	MR-TIM005
HisPur™ Ni-NTA Superflow Agarose	Thermo Fisher Scientific	25,214
Deposited data		
Mass spectrometry data	PRIDE	accession: PXD034098
Recombinant DNA		
pVL1393 Human CDK1	Brown et al., 2015 ³⁴	N/A
pET28-a Human cyclin B1(165-433), C167S/C238S/C350S	Petri et al., 2007 ⁶⁸	N/A
pET3-d Bovine cyclin A2 (170-430)	This paper	N/A
pGEX6P-1 Human CKS1 (5-79)	This paper	N/A

(Continued on next page)

Continued

REAGENT or RESOURCE	SOURCE	IDENTIFIER
Software and algorithms		
MaxQuant v1.6.14	https://maxquant.org/	N/A
WebLogo	https://weblogo.berkeley.edu/logo.cgi	N/A
DAVID enrichment analysis	https://david.ncifcrf.gov/	N/A
Other		
Dulbecco's Modified Eagle Medium (DMEM)	Life Technologies	10,565,018
Roswell Park Memorial Institute (RPMI)	Life Technologies	61,870,010
Dulbecco's phosphate buffered saline (DPBS)	Life Technologies	14,190,250
Fetal bovine serum	Life Technologies	10,270,106
Insect-Xpress insect cells medium	Lonza	BELN12-730Q
GeneJuice® Transfection reagent	Merck Millipore	70,967
Elutriation chamber	Beckman-Coulter	356,943
Sep-Pak 50 mg C ₁₈ columns	Waters	WAT054955
NEST micro-spin C ₁₈ columns	Harvard Apparatus	74-4601
HPLC 1 mm, 13 µm BEH resin C ₁₈ columns	Waters	186,002,346
24 mL Superdex 75 10/300 gel filtration column	Cytiva	29,148,721
53 mL Sephadex G-25 HiPrep 26/10 desalting column	Cytiva	10,470,505

RESOURCE AVAILABILITY

Lead contact

Further information and requests for resources and reagents should be directed to and will be fulfilled by the lead contact, Tony Ly, tly@dundee.ac.uk.

Materials availability

No new materials were generated. Materials are either commercially available, were produced using published protocols, or were obtained from collaborators.

Data and code availability

All data reported in this paper will be shared by the [lead contact](#) upon request. This paper does not report original code. Any additional information required to reanalyze the data reported in this paper is available from the [lead contact](#) upon request. Raw mass spectrometry data have been deposited to ProteomeXchange partner PRIDE with identifier PXD034098.

EXPERIMENTAL MODEL AND SUBJECT DETAILS

The following cell lines were used in this study: TK6 (human lymphoblast, gift from Earnshaw group). Cells were determined to be mycoplasma-free by a commercial ELISA-based detection kit.

METHOD DETAILS

Cell culture and centrifugal elutriation

TK6 cells were seeded at 80,000 cells/mL in 50 mL of Roswell Memorial Park Institute (RPMI) tissue culture medium supplemented with 10% Fetal Bovine Serum (FBS) in eight 15 cm dishes. After 48 h, cells were centrifuged, pooled, washed once in Dulbecco's Phosphate Buffered Saline (DPBS), and resuspended in 1% formaldehyde. Cells were mixed on a rotator at room temperature for 10 min. Cells were washed in DPBS and permeabilized in 90% methanol for a minimum of 24 h at −20°C. For centrifugal elutriation, methanol was removed, and cells were resuspended in elutriation buffer (5 mM MES, 100 mM NaCl, 1% FBS) and placed in elutriation chamber fitted into ultra-centrifuge. Cells were trapped in the elutriation chamber at 2010 rpm and 15 mL/min flow driven by a peristaltic pump. Cell size fractions were collected by progressively increasing the flow rate up to 35 mL/min. The cell cycle phase distribution of each elutriation fraction was analyzed by staining cells with propidium iodide (50 µg/mL RNase A, 50 µg/mL Propidium Iodide in DPBS) for 30 min prior to flow cytometry analysis. Fractions were combined in DPBS supplemented with 1x PhosSTOP (Roche) to obtain pooled fractions enriched in either 2N or 4N DNA content. A sample of cells was immunostained with H3pS10 antibody conjugated to Phycoerythrin (PE) for 30 min. Cells were washed once and resuspended in flow buffer containing 5 µg/mL DAPI.

To arrest cells in mitosis, TK6 cells were seeded at 800,000 cell/mL in RPMI supplemented with 10% FBS and 25 μ M STLC. After 16 h, cells were then harvested, fixed and permeabilized as described above.

To quantitate endogenous phosphatase activity post-fixation, 2 million fixed and permeabilized cells from elutriation fractions with 4N DNA content were incubated at 30°C with 50 mM para-nitrophenylphosphate in 150 μ L of phosphatase master-mix (50 mM HEPES, 100 mM NaCl, 10 mM MnCl_2) in the presence of either microcystin, PhosSTOP or 1 U of λ Phosphatase. Cells were then centrifuged, and supernatant was collected where the amount of para-nitrophenyl was estimated by measuring the absorbance at 405 nm.

Protein expression and purification

Full-length human CDK1 was expressed in insect cells from pVL1393 as a 3C-protease cleavable GST fusion, which leaves a short cloning artifact (GPLGS) at the N terminus. This construct was expressed, purified and phosphorylated (using GST-CAK1) as previously described^{34,69}. T161 phosphorylated CDK1 was then purified from GST-CAK1 by size exclusion column chromatography (SEC) on a Superdex 75 26/60 column equilibrated in 50 mM Tris pH7.5, 150 mM NaCl, 0.5 mM TCEP. Human Cyclin B1, residues 165–433 carrying the C167S/C238S/C350S mutations, was expressed in recombinant *E. coli* cells and purified as described exploiting the thrombin-cleavable hexahistidine tag encoded by the pET28-a (+) vector.⁶⁸ Human Cks1 was expressed from pET21a in *E. coli* cells and purified as described.³⁴ Bovine Cyclin A2, residues V170–V430 was expressed in *E. coli* Rosetta2 (DE3) pLYS-S cells as a GST-fusion from a modified pET3-d vector. It was purified by affinity purification followed by 3C cleavage to remove the GST tag and then a subsequent SEC step (Superdex 200 16/60 column). The bovine Cyclin A2 has the GPLMKY sequence at the N-terminus as a cloning artifact following 3C cleavage. As previously described,⁷⁰ bovine Cyclin A2 was purified in buffer containing MgCl_2 (300 mM NaCl, 100 mM MgCl_2 , 50 mM Tris-HCl, pH 8.0, 1 mM DTT) to help prevent aggregation.

To prepare the binary Cyclin B1-T161pCDK1 (BC) and ternary Cyclin B1- T161pCDK1-Cks1 (BCC) complexes, components were individually purified and then mixed in molar excesses of Cyclin B1 and Cks1 over CDK1 as required, and essentially as described.³⁴ The interaction between CDK1 and Cyclin B1 is dependent on the concentration of salt in the buffer. In each case, the final step to assemble the complex was carried out on a Superdex 75 HR26/60 SEC column equilibrated in modified Tris-buffered saline (TBS) containing 1.0 M NaCl, 50 mM Tris-HCl, pH 8.0, 1 mM DTT. Cyclin A2-T161pCDK1 (AC) was prepared by mixing purified phosphorylated CDK1 with an excess of purified bovine Cyclin A2 and separating the complex by SEC on a Superdex 75 HR26/60 column equilibrated in 50mM Tris pH 8.0, 200mM NaCl, 1mM DTT. For each purification, fractions containing the desired complex were pooled and concentrated to circa 10–12 mg mL⁻¹ by ultrafiltration and then fast frozen in aliquots in liquid nitrogen before storage at –80°C.

Purification of Aurora B-INCENP was carried out as described earlier.⁷¹

In vitro kinase assays on fixed cells

To induce protein phosphorylation *in vitro*, 2 million fixed and permeabilized TK6 cells from the pooled elutriation fractions above were blocked in 40 mM Tris (supplemented with 5% BSA and 1x PhosSTOP) for 10 min. Cells were then washed by centrifugation at 15,000 g for 30 s and placed in 400 μ L of phosphorylation master-mix (40 mM Tris, pH 7.5; 0.5% BSA, 10 mM ATP, 1x PhosSTOP and recombinant CDK1 complexes) for 40 min at room temperature. For phosphorylation with Aurora B, cells were blocked in DPBS (Supplemented with 5% BSA and 1x PhosSTOP) for 10 min on ice then placed in a master-mix (DPBS, 0.5% BSA, 10 mM ATP, 1x PhosSTOP and recombinant Aurora B) for 40 min at 37°C. To stop the phosphorylation reactions, cells were quenched by washing three times with 11 mM EDTA in either 40 mM Tris (Supplemented with 0.5% BSA) for assays with CDK1 or in DPBS (Supplemented with 0.5% BSA) for assays with Aurora B. Cells were then resuspended in 300 μ L of ice-cold DPBS containing 1x PhosSTOP. To check the *in vitro* phosphorylation by western blotting, 200 μ L of this suspension was placed in a new tube, centrifuged and pellets were resuspended in 70 μ L cell extraction buffer (1 mM HEPES, 10 μ M EDTA, 2% SDS, 1x cCOMPLETE protease inhibitor cocktail and 1x PhosSTOP). Extracts were then sonicated for 30 s at 10% amplitude, and crosslinking was reversed by heating at 95°C for 50 min. Proteins in the lysates were then reduced by adding 25 mM TCEP and mixed with 25 μ L of LDS sample buffer for loading. Proteins were separated by SDS-PAGE at 150 V in 1x NuPAGE MES Running Buffer for 2 h and transferred onto 0.2 μ m nitrocellulose membranes at 0.2 A in 80% NuPAGE MES buffer +20% methanol (v/v) for 2 h. Membranes were stained overnight with anti-Phospho-SPX [KR] motif and anti-Alpha-Tubulin antibodies in TBS (Supplemented with 5% BSA) at 4°C. This was done after blocking with TBS (Supplemented with 5% milk) for a minimum of 1 h. To remove the primary antibodies, membranes were washed three times with TBS-T (TBS and 0.1% Tween) for 5 min each. Secondary antibodies conjugated to IRDye680 or IRDye800 in TBS (Supplemented with 5% BSA) were then added for 1–2 h at room temperature and bands were visualized by scanning the membranes with Li-COR Odyssey instrument.

In the experiments where cells were subjected to sequential phosphatase then kinase reactions, 2 million cells from the elutriation fractions above were preincubated for 16 h with 800 U of λ Phosphatase in phosphatase master-mix (Supplemented with 0.5% BSA). To stop the reactions, cells were washed three times with DPBS then heated for 40 min at 65°C. Cells were then blocked and *in vitro* phosphorylations were carried out as described above.

Sample preparation for TMT phosphoproteomic analysis of fixed cells

To prepare peptide digests from fixed cells, 100 μ L of cells from above were washed by centrifugation, resuspended in digestion buffer, which consisted of: 100 mM triethyl ammonium bicarbonate (TEAB), 2 mM MgCl_2 and 5 U Benzonase; pH 8.5. Nucleic acids were digested at 37°C for 30 min.⁴⁶ Proteins were then digested by adding 1.25 μ g Trypsin protease for 16 h at 37°C followed by

another addition of 1.25 μ g trypsin for 4 h. Peptides were then acidified by adding formic acid to a final concentration of 2% and desalted using NEST C_{18} micro-spin columns. Briefly, peptides were bound to C_{18} columns that were previously conditioned with 100% acetonitrile and equilibrated with 0.5% formic acid. Columns were then washed twice with 0.5% formic acid and peptides were eluted with 80% acetonitrile diluted in 0.5% formic acid. To remove solvent, samples were dried at 30°C until fully dry. Peptides were resuspended in 50 μ L of 100 mM TEAB and mixed with 0.25 mg of TMTpro from a set of 16 plex resuspended in 10 μ L acetonitrile for 1 h. The isobaric labeling reaction was then quenched by adding 2.5 μ L of 5% hydroxylamine to these samples for 15 min at 37°C. Peptides from samples in the following experiments were pooled together: AC/BC titration experiment discussed in Figures 1 and 2; BCC and BC titration experiment in Figure 3. The experiment involved λ Phosphatase pre-treatment of fixed cells in Figure 4 was pooled in the same TMT set with samples for CCR sites identification discussed in Figure 5 and the identification of mitotic CCR sites that were Cks1 dependent was done with the same samples used for identifying the priming phosphorylation kinase in Figure 4. Peptides from each pool were then dried, resuspended in 0.5% formic acid, and divided into two fractions each was desalted in a 50 mg Sep-Pak C_{18} column. To remove free TMT from samples, an extra wash with 0.5% acetic acid was added to the protocol and elution was done in 80% acetonitrile, this time diluted in 0.5% acetic acid. Samples were phosphoenriched by mixing peptides with 3.2 mg of MagReSyn Ti-IMAC in load buffer, which consisted of 80% acetonitrile, 5% trifluoroacetic acid (TFA) and 5% glycolic acid, for 20 min at 25°C. Beads were washed for 2 min with 80% acetonitrile +1% TFA. This was followed by two 2 min washes in 10% acetonitrile +0.2% TFA. Phosphorylated peptides were eluted in 1% ammonium hydroxide for 15 min twice in elution buffer. This was followed by a second elution for 1 h in a 50/50 mix of 1% ammonium hydroxide and acetonitrile (v/v). To increase the number of phosphorylated peptides identified, the flow through was dipped in a new batch of MagReSyn Ti-IMAC beads and the phospho-enrichment step was repeated as described above. 5% of the pooled peptides were kept without phosphoenrichment for total proteome analysis. To remove any residual magnetic beads, peptides were dried and desalting with NEST micro-spin C_{18} columns was performed as described above. For deep phosphorylation analysis, peptides were fractionated using high pH reverse phase HPLC. Briefly, peptides were passed through a 1 mm column packed with 13 μ m sized BEH silica resin coated with C_{18} and were eluted with a gradient of 15–80% B, with the following A and B mobile phases: 10 mM ammonium formate pH 9.3, 10/90 mixture of 10 mM ammonium formate pH 9.3 and 100% acetonitrile. Peptides were eluted into 16 wells, dried and stored at –20°C until data acquisition by mass spectrometry.

Proteomics data analysis

In the kinase assay where phosphorylation by BC was compared to BCC described in Figure 3, the TMTpro labeled and phosphoenriched samples were analyzed using Dionex Ultimate 3000 HPLC-Coupled Tribrid Fusion Lumos mass spectrometer. Samples were loaded and separated using 75 μ m \times 50 cm EASY-Spray column with 2 μ m sized particles, which was assembled on an EASY-Spray source and operated constantly at 50°C. Two mobile phases were used to separate the peptides: Phase A consisting of 0.1% formic acid in LC-MS grade water and phase B consisting of 80% acetonitrile and 0.1% formic acid. Peptides were loaded onto the column at a flow rate of 0.3 μ L/min and eluted at a flow rate of 0.25 μ L/min according to the following gradient: 2 to 40% mobile phase B in 120 min and then to 95% in 11 min. Mobile phase B was retained at 95% for 5 min and returned back to 2% a minute after until the end of the run (160 min in total for each fraction). A voltage of 2.2 kV was set when spraying this gradient of peptides into the front end of the mass spectrometer at ion capillary temperature of 280°C with a maximum cycle time of 3 s. An MS1 scan at a resolution of 120,000 in Orbitrap detector was performed with a maximum injection time of 50 msec and the top 10 most abundant ions within a scan range of 380–1500 m/z based on the m/z signal with charge states of 2–6 from that scan were chosen for fragmentation in an HCD cell at 28%. This was followed by a rapid MS2 scan on a linear ion trap for peptide identification with a maximum injection time of 50 msec. To minimize the TMTpro reporter ion ratio distortion, 5 precursor fragments were selected for a synchronous precursor selection (SPS) MS3 method from 3 precursor dependent scans.⁷² These fragments were further fragmented at 55% collision energy in an HCD chamber and analyzed using an Orbitrap detector at a resolution of 55,000 with a 90 msec maximum injection time. The samples from this experiment that were not phosphoenriched were analyzed for total proteome analysis using the same method, except that the MS2 fragmentation was performed in a CID cell at 35% energy.

In the experiment where AC and BC phosphorylation of fixed cells was compared (Figure 1), both total and phosphorylated peptides were loaded into a trap column (100 μ m \times 2 cm, PepMap nanoViper C_{18} column, 5 μ m, 100 Å) attached to a Dionex Ultimate 3000 RS system in 0.1% TFA for 3 min and then separated through analytical column (75 μ m \times 50 cm, PepMap RSLC C_{18} column, 2 μ m, 100 Å) in the following mobile phases: 0.1% formic acid (Solvent A) and 80% acetonitrile +0.1% formic acid (Solvent B). Separation was carried out using a linear solvent gradient of 5%–35% for 130 min followed by a steep gradient to 98% up until 152 min after which the solvent concentration was dropped back to 5%. The separation was carried out at a flow rate of 300 nL/min. Peptides were then sprayed into the front end of a Tribrid Fusion mass spectrometer through a nanoelectrospray ionizer with a cycle time of 3 s and the MS1 data for precursor ions were acquired in an Orbitrap detector at a resolution of 120,000. The top 10 most abundant peaks with charge states of 2–6 were then fragmented in an HCD chamber at 28% and analyzed on a linear ion trap for peptides identification in a maximum injection time of 70 msec. SPS MS3 was then performed on the top 5 precursor fragments from 5 precursor dependent scans following HCD fragmentation (58%) in Orbitrap detector at a resolution of 50,000 with a maximum injection time of 110 msec.

Finally, phosphorylated and total samples that involved sequential reactions with phosphatase and CDK1 described in Figure 4 and those used for the analysis of CDK1 CCR sites described in Figure 5 were labeled with TMTpro and pooled into the same set and analyzed on an Orbitrap Eclipse mass spectrometer. Peptides were initially trapped in PepMap nanoViper C_{18} column

(100 μm \times 2 cm, 5 μm , 100 \AA) in 0.1% TFA for 5 min then fractionated with analytical PepMap RSLC C₁₈ column (75 μm \times 50 cm, 2 μm , 100 \AA) on a Dionex Ultimate 3000 RS system with a 5%–35% gradient for 130 min. This was followed by a steep increase in solvent concentration to 98% for up to 152 min then a drop to 5% for 1 min. Peptides from the gradient were injected into the front end of a Tribrid Eclipse mass spectrometer through a nanoelectrospray ionizer in a 3 s cycle time. Precursor ions were detected in a master scan using Orbitrap detector at a resolution of 120,000 with a maximum injection time of 50 msec. Precursor ions with top 10 signals and charge states of 2–7 were selected for fragmentation using HCD (28%) and analyzed by a linear ion trap with a maximum injection time of 50 msec. SPS MS3 of 5 fragments from 5 precursor dependent runs were fragmented by HCD (55%) and analyzed by Orbitrap at a resolution of 50,000 with a maximum injection time of 90 msec.

Raw data from the assays on fixed cells were processed on MaxQuant version 1.6.14.⁷³ To perform motif enrichment analysis, sequences of each cluster were inserted into the online tool WebLogo and plots generated were used in the [results](#) section presented here.⁷⁴ For motif enrichment analysis with Icelogo, the sequences in the cluster of interest were inserted as the positive set and sites in either the rest of the heatmap or in the rest of the phospho-proteome were inserted as the background.⁷⁵ To match the CCR sites with the *in vitro* data, a column containing the gene name, the phosphorylated residue, and the location of that residue in the protein was added to the two tables. Rows with matching data in that column in both tables were considered *in vitro* targets of CDK1 with CCR endogenous phosphorylation. To perform GO analysis, gene names for each dataset were inserted into DAVID Bioinformatics (<https://david.ncifcrf.gov>) and fold enrichments generated by the online tool were used to plot functional annotations and subcellular localizations of proteins within that dataset.

***In vitro* kinase assays on recombinant proteins**

NDC80^{Broccoli} was purified as described previously.⁷⁶ Cyclin H-CDK7-MAT1 was purchased from the MRC-Protein Phosphorylation and Ubiquitylation Unit Reagents and Services at University of Dundee (clone DU49574) and PML-IV was a generous gift from Ronald T. Hay, Anna Plechanovova and Ania Eugui Anta at the Center for Gene Regulation and Expression, University of Dundee. For phosphorylation reactions, 500 nM of recombinant NDC80^{Broccoli}, PML-IV or Cyclin H-CDK7-MAT1 were incubated at 21°C with 100 nM of AC, BC or BCC for 40 min in 40 mM Tris buffer, pH 7.5 and 10 mM ATP. Reactions were then stopped by adding 2% SDS and samples were reduced by adding 25 mM TCEP for 10 min at 37°C then alkylated with 25 mM iodoacetamide for 1 h in the dark. To remove SDS from the samples, proteins were precipitated by three rounds of acetone washing and pelleting at 4°C followed by a single wash with 90% ethanol to remove residual acetone. Samples were then dried for 10 min and resuspended in 50 μL TEAB, and tryptic digestion was carried out as described above. Peptide digests were acidified using 1% TFA then bound to stage C₁₈ columns before being eluted in 80% acetonitrile diluted in 0.1% TFA. To further clean up the samples, desalted peptides were resuspended in 50 mM ammonium bicarbonate supplemented with 0.05% formic acid, pH 7 and incubated with HiPPR beads according to manufacturer's instructions. Eluted peptides were dried down, resuspended in 1% formic acid and injected into a Tribrid Fusion mass spectrometer as described for samples in [Figure 1](#), using a 47 min chromatography in C₁₈ analytical column with a solvent gradient of 5%–98% in 38 min. MS1 and MS2 scans were performed using similar acquisition methods, but with a maximum injection time of 50 msec for MS2 and without MSA or SPS MS3. Peptides were identified using MaxQuant and their phosphorylation was quantitated with Skyline.⁷⁷ ppm was calculated by dividing the phosphorylation intensity of a particular peptide by that of the entire sample and multiplying the results by 10⁶.

QUANTIFICATION AND STATISTICAL ANALYSIS

To normalize the mass spectrometry data, reporter intensities for histone proteins detected in all TMTpro channels in the Protein Groups file were summed. Summed intensities were used to normalize the reporter ion intensities for sites in the corresponding TMTpro channels in the PhosphoSTY file to adjust for mixing error. The fold change in phosphorylation intensity for each site was then calculated by dividing the normalized reporter ion intensity of that site in the sample treated with the active recombinant kinase by its normalized reporter ion intensity in the control sample. An arbitrary value of one was added to sites with missing values in the control (kinase-dead) sample. Sites with at least 2-fold increase in their phosphorylation were considered *in vitro* phosphorylated. To perform clustering based on the phosphorylation pattern, the fold change for each site in a particular channel was scaled, i.e. $(x - \bar{x})/s$, where s is the sample standard deviation and \bar{x} is the sample mean. Data were then plotted on a heatmap and sites with missing values were eliminated. K-means clustering was then used to segregate sites with similar phosphorylation changes into clusters using the Ward agglomeration algorithm. Regular expressions were used to grep sites with certain amino acid sequences, such as those with or without a +1 proline or those within the [ST][P]X[KR] motif.

For multisite phosphorylation analyses, the location of phosphorylated residues was identified using the 'Modification window' column in the PhosphoSTY file. A value of 1 or 0 were assigned for phosphorylated and non-phosphorylated sites within that column, respectively. Multisite phosphorylation and phosphosite proximity on the substrate were assessed by calculating the sum of residues with 1 value and the number of sites that separated these phosphorylated residues, respectively.

Definitions of dispersion measures used, and n (biological repeats from independent cell line cultures), are provided in the figure legends.